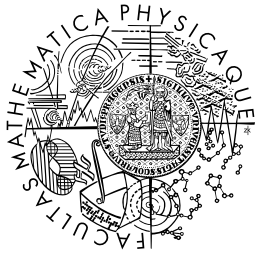

FACULTY
OF MATHEMATICS
AND PHYSICS
Charles University

BACHELOR THESIS

Pavel Šklíba

Calculations of photoelectron spectra of small water clusters using the independent molecule model

Institute of Theoretical Physics

Supervisor of the bachelor thesis:	Mgr. Zdeněk Mašín, Ph.D.
Study programme:	Physics
Study branch:	General Physics

Prague 2020

I declare that I carried out this bachelor thesis independently, and only with the cited sources, literature and other professional sources.

I understand that my work relates to the rights and obligations under the Act No. 121/2000 Sb., the Copyright Act, as amended, in particular the fact that the Charles University has the right to conclude a license agreement on the use of this work as a school work pursuant to Section 60 subsection 1 of the Copyright Act.

In Prague, date 30th July 2020 Pavel Šklíba

I dedicate this thesis to my love since I am grateful to her for that she is always there for me. I also would like to thank my parents for their support and especially my supervisor Mgr. Zdeněk Mašín, Ph.D. for his patience with me, huge help with this thesis and all the things I have learned throughout this work.

Title: Calculations of photoelectron spectra of small water clusters using the independent molecule model

Author: Pavel Šklíba

Institute: Institute of Theoretical Physics

Supervisor: Mgr. Zdeněk Mašín, Ph.D., Institute of Theoretical Physics

Abstract: The aim of this thesis is to investigate theoretically photoelectron spectra of small water molecular clusters. This work is motivated by the recent experimental results of Hartweg et al [Phys. Rev. Letters **118**, 103402, 2017] which showed that with an increasing number of constituent molecules in the water cluster the asymmetry parameter characterizing the photoelectron angular distribution converges to a universal shape. At the moment there are no theoretical calculations to support this finding. Therefore, we have developed a very simple model of photoionization of molecular clusters based on the use of photoionization data for a single molecule. We have found that the results of our model are sensitive to the different conformations of the clusters. Some of our results for the photoelectron angular distribution exhibit trends observed in the experiment. Nevertheless, the validity of our model will have to be studied in the future with the help of accurate calculations before the results can be conclusively interpreted.

Keywords: photoionization, asymmetry parameters, cross section, quantum interference, water molecular clusters, molecular structure

Contents

Introduction

Molecular clusters are ensembles of molecules bound together by intermolecular forces such as e.g. hydrogen bonding or dipole–dipole interaction, but not by covalent bonds (Johnston [2002], ch. 3). Such clusters in general can vary in size and can be composed of molecules of the same type (homogeneous) or of multiple different types (heterogeneous). The character and physical properties of the molecular clusters are typically different from those of single molecules or gas, liquid or bulk solid of the same chemical substance (Caprasecca [2010], p. 4). Note that so called cluster molecules which are bound by covalent bonds are not the molecular clusters in this sense.

Clusters of various types and substances, including water clusters, are present in many different environments, such as the atmosphere of Earth (Harrison and Carslaw [2003]), interstellar clouds (Duley [1996]), dense gaseous media (Kreil et al. [1998]) or biological structures (Nam et al. [2007], Freitas et al. [2009]). In each of these environments the clusters are created by different main processes. In the atmosphere clusters are produced by the charge driven reactions of polar molecules with other molecules of the atmosphere ionized by the cosmic rays (Harrison and Carslaw [2003]). These atmospheric molecular clusters continue to grow into aerosols which then start the nucleation of water droplets that later form clouds and fogs and affect a vast number of other processes in the atmosphere (Morrell and Shields [2010], Castleman and Jena [2006]). In space, clusters are formed from molecules released from solid surfaces after impacts of ions or electrons. In dense gases they form spontaneously (Kreil et al. [1998]) and thus they are often studied in this environment.

In biological environments, clusters are very important for chemical reactions, and for structural stabilization and they affect processes leading to radiation damage of biochemical structures (Caprasecca [2010], p. 5). For example water clusters are probably responsible for the structure of the hydration layers surrounding some biomolecules, including DNA (Yonetani et al. [2008], Sen et al. [2009], Dragan et al. [2009]). There are even clusters of biomolecules, which also behave differently then isolated molecules of the same type (Nam et al. [2007], Freitas et al. [2009]).

Focusing on water clusters from now on, it must be pointed out that besides these biological structures $(H_2O)_n$ clusters are also present in all the other environments mentioned above and take part in many more specific processes that are not mentioned here (see e.g. Fárník [2011] or Johnston [2002]), which makes them very important for biology, meteorology and many other fields. That is the reason why there has been a lot of effort to study these clusters experimentally and theoretically.

In laboratory conditions, water clusters can be studied in dense gaseous media, where they form spontaneously (Caprasecca [2010]) as mentioned above, or they can be created artificially by supersonic jet expansion in molecular beams (Fárník [2011]). This technique is capable of preparing molecular clusters with well defined size distributions (number of molecules), typically exponential or log-normal, which depends on the form of expansion of the molecular gas into the vacuum. However, the exact structure of the clusters created in the molecular

beam is practically beyond control. And that is the main motivation for this thesis and its main goal – to theoretically investigate (under certain approximations) the possibilities of analysing the specific structure of small $(H_2O)_n$ water clusters (with small number of molecules n) using so called photoelectron spectroscopy.

According to Johnston [2002], section 3.3, most of the spectroscopic studies of water clusters were focused either on infrared (see e.g. Huisken et al. [1996]) or microwave spectroscopy, electron diffraction or mass spectroscopy. Some of them even studied the specific geometric structure of the small or large water clusters (see Johnston [2002], section 3.3.4, in particular paragraph 3.3.4.3 discussing the $(H_2O)_6$ cluster), mostly combining the spectroscopic measurements and ab initio theoretical calculations of the ground state structures of the water clusters.

Recently, photoionization spectroscopy has been established as an important tool for studies of molecular clusters. There are some works on the photoelectron spectroscopy of water clusters, both small (Hartweg et al. [2017]) and larger (see Zhang et al. [2013] or Trabattoni et al. [2020]). In these cases, what is being analysed are the electrons released by ionizing the cluster by absorption of a single photon. If linearly polarized light is used, the angular distribution of the photoelectrons is

$$I \sim 1 + \beta(E) P_2(\cos\theta'), \tag{1}$$

where $\beta(E)$ is the asymmetry (or anisotropy) parameter, E is the photon energy and P_2 is the second order Legendre polynomial. The angle θ' is measured with

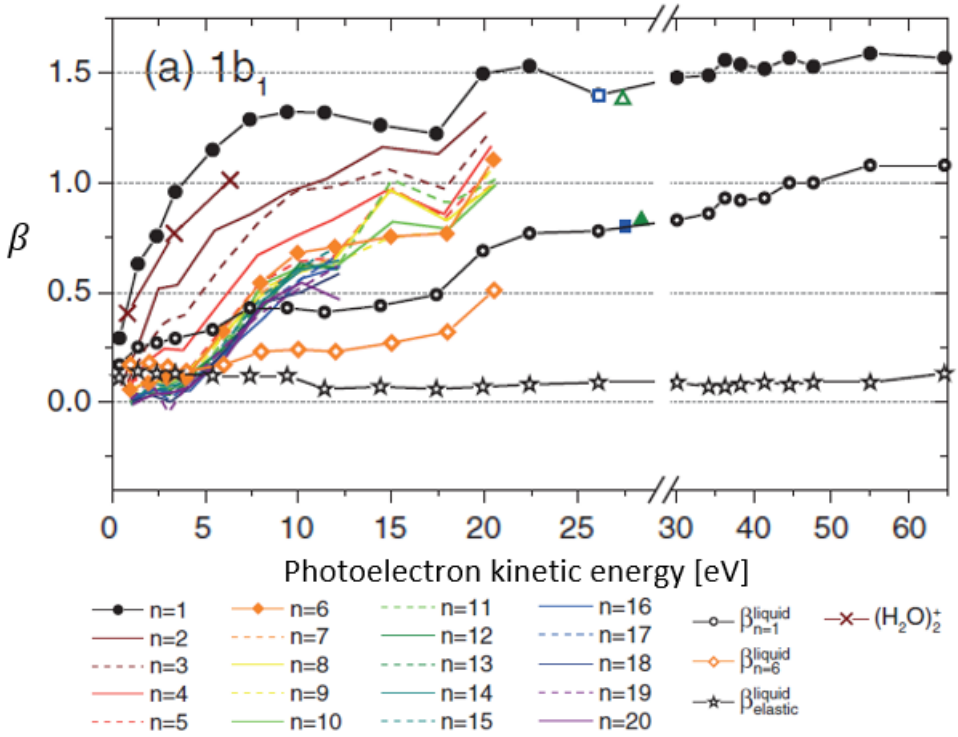

Figure 1: Adapted from Hartweg et al. [2017]. Experimental β-parameter for the photoionization of the $1b_1$ molecular orbital for isolated H_2O molecule, small $(H_2O)_n$ clusters with $2 \leq n \leq 20$, $(H_2O)_2^+$ ions and calculated predictions for liquid water. The green triangles show the results of Zhang et al. [2013] for larger clusters and blue squares show the results of Faubel et al. [2012] for liquid water.

respect to the direction if the electric field vector, identified with the z' axis of the lab frame.

Hartweg et al. [2017] measured the asymmetry parameters of the photoelectron angular distribution for photoionization of three molecular orbitals of H_2O molecules – orbitals $1b_1$, $3a_1$ and $1b_2$ – for isolated H_2O monomers and small $(H_2O)_n$ clusters of 2-20 molecules. The main result of Hartweg et al. [2017], see fig. 1, is the observation of a gradual "convergence" of the photoelectron angular distribution from that for a single molecule to that of bulk (liquid) water with clusters forming the intermediate step. This especially holds for "the outermost" orbitals $1b_1$, $3a_1$ for which the curves of the β-parameters systematically decrease with increasing number of molecules n and converge to a universal curve at about $n \sim 5$ or 6. Zhang et al. [2013] got a similar trend of decrease of the β-parameter also for larger water clusters. Currently there are no theoretical calculations of the photoelectron distributions to support these observations.

As an explanation for that trend for larger clusters, Zhang et al. [2013] and Hartweg et al. [2017] propose the effect of multiple scattering of the photoelectrons in the cluster. In this thesis, this effect will be neglected, though only small, not large clusters will be studied here. One of the possible explanations for the trend of decreasing β and the change in its shape for small water clusters is an "interference of partial waves from many centers" of photoionization, see p. 3 of Hartweg et al. [2017].

The main goal of this thesis is to formulate a theory of photoionization of water clusters in the approximation of independent molecules, which includes the effect of multicenter ionization, and investigate whether this model explains some of the experimental results obtained by Hartweg et al. [2017]. Besides

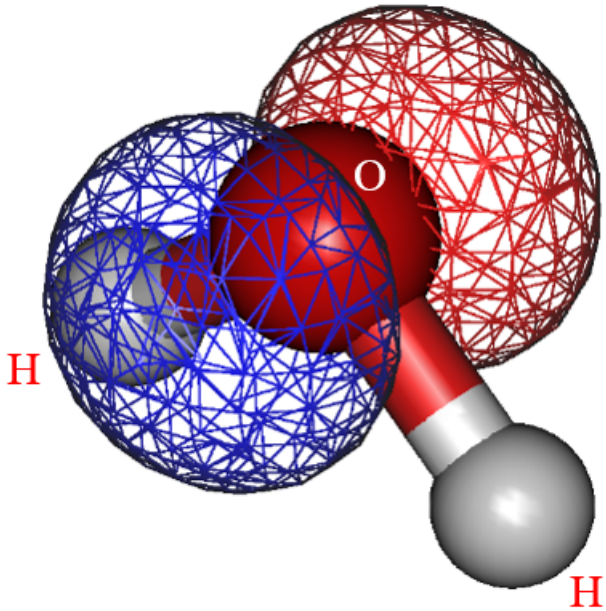

Figure 2: The $1b_1$ molecular orbital of an H_2O molecule that we focus on in this thesis. The oxygen atom is red, the hydrogen atoms are white. The visualization was made by the code Gabedit (see e.g. Allouche [2011]) and provided to me by my supervisor.

that, we will also investigate the effects of the cluster conformation, especially of the orientations of the individual H_2O molecules with respect to the cluster, in order to see whether the photoelectron spectroscopy could be used to verify the theoretically calculated cluster geometries.

The putative geometric structures of small water clusters will be taken from the recent work Rakshit et al. [2019a]. The authors used "an improved version of the Monte Carlo Temperature Basin Paving (MCTBP) method" (Rakshit et al. [2019b]) together with an interaction potential labeled as TTM2.1-F for clusters composed of 3-30 H_2O molecules. The resulting most probable geometries are freely accessible in the database on the website (Rakshit et al. [2019b]).

The tests of the method developed here will focus only on the $1b_1$ molecular orbital of an H_2O monomer (see figure 2). This orbital has the advantage that it is very close to the atomic p-orbital which provides a fast convergence of the partial wave expansion. The input data for that orbital needed for calculations were given to me by my supervisor.

1. Theory

The theory of photoionization is a part of the quantum theory of particle collisions. The probability amplitude of photoionization can be calculated using the non-stationary perturbation theory, considering the electromagnetic waves as a classical external periodic-field perturbation added to the Hamiltonian (see Friedrich [2006], chapter 2.4 or Cejnar [2013], p. 149-157). This approach leads to the expression of the probability amplitude in terms of the dipole matrix elements between the initial (neutral) and final (ionic) wave functions of the system. Manipulating these dipole matrix elements will be the central task of the theory developed here.

This theory will be briefly summarized in Subsection 1.2.1 bellow, and after that, a mathematical description of the photoelectron angular distribution for a single molecule and its generalization for a cluster will be derived.

Unless explicitly stated, atomic units (a.u.) will be used in the entire thesis. These units are defined by setting the following fundamental constants to unity:

$$\begin{aligned} \text{Planck constant (reduced):} \quad & \hbar = 1, \\ \text{elementary charge:} \quad & e = 1, \\ \text{electron rest mass:} \quad & m_e = 1, \\ \text{Bohr radius:} \quad & a_0 = 1. \end{aligned} \tag{1.1}$$

The atomic unit of energy is Hartree defined as:

$$E_h = \frac{\hbar^2}{m_e a_0^2} = 27.2113961 \text{ eV}, \tag{1.2}$$

where eV denotes electronvolts. For the cross sections, which have the units of area, we adopt the megabarn units (Mb):

$$1 \text{ Mb} = 10^{-22} \text{ m}^2. \tag{1.3}$$

1.1 General form of the photoelectron angular distribution

Since the orientation of molecules or clusters produced by a molecular beam with respect to the lab frame usually cannot be fixed, the theory is forced to work with randomly oriented molecules and clusters. Therefore, the differential cross section of the photoelectron angular distribution must be averaged over all orientations of the molecules or clusters (see e.g. Chandra [1987]), i.e. integrated over all their Euler angles defined with respect to the lab frame.

Angular distributions of the products of binary reactions were first studied generally by Yang [1948]. A special case of the general binary reaction is the ionization of a molecule by a single photon:

$$M + h\nu \longrightarrow M^+ + e^-. \tag{1.4}$$

In this case Yang's theorem implies that the photoelectron angular distribution has the form:

$$\left(\frac{\mathrm{d}\sigma}{\mathrm{d}\boldsymbol{k}'_f}\right)_{Av} = \frac{\sigma(E)}{4\pi}\left(1+\beta_1(E)P_1(\cos\theta')+\beta_2(E)P_2(\cos\theta')\right), \tag{1.5}$$

where $\left(\frac{\mathrm{d}\sigma}{\mathrm{d}\boldsymbol{k}'_f}\right)_{Av}$ is the averaged differential cross section, $\boldsymbol{k}'_f$ is the momentum vector of the photoelectron in the lab frame, here written in the sense that the differential cross section is measured with respect to the direction of $\boldsymbol{k}'_f$, $\sigma(E)$ is the integral cross section, $\beta_1(E)$ and $\beta_2(E)$ are the so called asymmetry parameters, mentioned already in the introduction, E is the photon energy, P_1, P_2 are the Legendre polynomials and θ' is the angle measured from the lab frame z'-axis.

The relation (1.5) actually holds for photoelectron angular distribution in general which means that the entire information about that distribution is contained in the total cross section $\sigma(E)$ and the asymmetry parameters $\beta_1(E)$ and $\beta_2(E)$. And moreover, the β_1 parameter is nonzero only in photoionization of chiral molecules (i.e. molecules that don't have a plane of symmetry) by circularly polarized light, see Ritchie [1976]. Therefore in many cases, all the information about the angular distribution is included only in $\sigma(E)$ and $\beta_2(E)$. These properties are very important for both experimental and theoretical studies of the photoelectron spectroscopy.

The three parameters $\sigma(E)$, $\beta_1(E)$, $\beta_2(E)$ depend on the energy of ionizing photons which can be well controlled e.g. by using a monochromatic laser or a synchrotron. Hence these parameters can be obtained by measuring the energy and the angular distribution of photoelectrons in spectroscopic experiments, providing some information about the ionized material.

The observables σ, β_1, β_2 are functions of the quantum transition amplitudes (the dipole matrix elements). In the following sections we will provide derivation of these observables first for a single molecule and then for a cluster.

1.2 Photoionization of a single molecule

Since the derivation of the photoionization amplitude is not the main subject of this thesis, only its main ideas will be presented here. For a detailed derivation see e.g. Friedrich [2006], section 2.4. Application of the first order perturbation theory and the dipole approximation leads to the expression of the photoionization amplitude in terms of the dipole matrix elements as mentioned above (see e.g. Friedrich [2006], p. 131 or Cejnar [2013], p. 156). The relation connecting the photoelectron angular distribution will be derived in detail using the partial wave expansion of these dipole matrix elements.

1.2.1 Photoionization amplitude of a single molecule

To describe a single photon ionization it is sufficient to consider the electromagnetic field as a classical external field. Then the non-relativistic Hamiltonian

describing interaction of N electrons with the field is[1]:

$$\hat{H} = \sum_{i=1}^{N} \frac{1}{2}[\hat{\mathbf{p}}_i - q\boldsymbol{A}(\hat{\mathbf{x}}_i, t)]^2 + \sum_{i=1}^{N} V(\hat{\mathbf{x}}_i, t), \tag{1.6}$$

where $\hat{\mathbf{p}}_i$ and $\hat{\mathbf{x}}_i$ are the momentum and coordinate vector operators of the i-th electron (Friedrich [2006], p. 125 or Cejnar [2013], p. 155). The potential $V(\hat{\mathbf{x}}_i, t)$ includes the scalar potential $\Phi(\hat{\mathbf{x}}_i, t)$ and all field-free interaction terms. Performing the square of the first term gives:

$$\hat{H} = \sum_{i=1}^{N} \left[\frac{\hat{\mathbf{p}}_i^2}{2} + V(\hat{\mathbf{x}}_i, t) \right] - \sum_{i=1}^{N} \frac{q}{2} \left[\boldsymbol{A}(\hat{\mathbf{x}}_i, t) \cdot \hat{\mathbf{p}}_i + \hat{\mathbf{p}}_i \cdot \boldsymbol{A}(\hat{\mathbf{x}}_i, t) + q\boldsymbol{A}(\hat{\mathbf{x}}_i, t)^2 \right]. \tag{1.7}$$

In the first order perturbation theory, the term $q\boldsymbol{A}(\hat{\mathbf{x}}_i, t)^2$ can be neglected (Friedrich [2006], p. 129, Cejnar [2013], p. 155), and furthermore, if we use the Coulomb gauge condition:

$$\nabla \cdot \boldsymbol{A}(\hat{\mathbf{x}}_i, t) = 0, \tag{1.8}$$

the fourth term in the Hamiltonian (1.7) vanishes too and so does the scalar potential since we assume a source-free field. Therefore, we can write:

$$\hat{H} = \sum_{i=1}^{N} \left[\frac{\hat{\mathbf{p}}_i^2}{2} + V(\hat{\mathbf{x}}_i) \right] - \sum_{i=1}^{N} \frac{q}{2} \boldsymbol{A}(\hat{\mathbf{x}}_i, t) \cdot \hat{\mathbf{p}}_i. \tag{1.9}$$

In this shape, the first two terms form the free Hamiltonian:

$$\hat{H}_0 = \sum_{i=1}^{N} \left[\frac{\hat{\mathbf{p}}_i^2}{2} + V(\hat{\mathbf{x}}_i) \right] \tag{1.10}$$

and the second term is identified as the perturbation:

$$\hat{H}_I = -\sum_{i=1}^{N} \frac{q}{2} \boldsymbol{A}(\hat{\mathbf{x}}_i, t) \cdot \hat{\mathbf{p}}_i. \tag{1.11}$$

To describe the photoionization we assume the electromagnetic wave in the form of a plane wave (Cejnar [2013], p. 156):

$$\boldsymbol{A}(\hat{\mathbf{r}}, t) = 2A_0 \boldsymbol{\xi} \cos\left(\frac{\omega}{c} \boldsymbol{n} \cdot \hat{\mathbf{r}} - \omega t \right) = A_0 \boldsymbol{\xi} \left[e^{+\mathrm{i}\left(\frac{\omega}{c}\boldsymbol{n}\cdot\hat{\mathbf{r}} - \omega t\right)} + e^{-\mathrm{i}\left(\frac{\omega}{c}\boldsymbol{n}\cdot\hat{\mathbf{r}} - \omega t\right)} \right], \tag{1.12}$$

where $\boldsymbol{\xi}$ is the polarization vector, $\boldsymbol{n}$ is the direction of propagation of the wave and ω is the angular frequency (i.e. the energy of the photon in atomic units). Inserting this expression into the equation (1.11) yields a periodic perturbation:

$$\hat{H}_I = -\frac{q}{2} A_0 \sum_{i=1}^{N} \left[e^{+\mathrm{i}\left(\frac{\omega}{c}\boldsymbol{n}\cdot\hat{\mathbf{r}}_i\right)} (\boldsymbol{\xi} \cdot \hat{\mathbf{p}}_i) e^{-\mathrm{i}\omega t} + e^{-\mathrm{i}\left(\frac{\omega}{c}\boldsymbol{n}\cdot\hat{\mathbf{r}}_i\right)} (\boldsymbol{\xi} \cdot \hat{\mathbf{p}}_i) e^{+\mathrm{i}\omega t} \right], \tag{1.13}$$

where the first term describes an absorption of the quantum of energy ω and the second term a stimulated emission (Cejnar [2013], p. 154-156):

$$\hat{V}^\dagger = q e^{+\mathrm{i}\frac{\omega}{c}\boldsymbol{n}\cdot\hat{\mathbf{r}}_i} (\boldsymbol{\xi} \cdot \hat{\mathbf{p}}_i), \tag{1.14}$$

$$\hat{V} = q e^{-\mathrm{i}\frac{\omega}{c}\boldsymbol{n}\cdot\hat{\mathbf{r}}_i} (\boldsymbol{\xi} \cdot \hat{\mathbf{p}}_i). \tag{1.15}$$

[1] Since we use the atomic units defined by eq. (1.1), we omit writing the symbol m_e. However we keep writing the charge $q = -e$, because it will be used bellow.

Therefore, when calculating the single photon ionization amplitude, only the absorption potential (1.14) from the first term in eq. (1.13) contributes.

The transition amplitude is calculated using Fermi's golden rule (Friedrich [2006], section 2.4.1, Cejnar [2013], p. 153) which assumes that the interaction has an infinite duration (the electromagnetic pulse is very long). In this approximation the photoionization amplitude will be proportional to the matrix element of the $\hat{V}^\dagger$ potential[2]:

$$a_{fi}^{\boldsymbol{\xi}}(\boldsymbol{k}_f) \propto \left\langle \Psi_{f,\boldsymbol{k}_f}^{(-)} \middle| q \sum_{j=1}^{N} e^{+\mathrm{i}\frac{\omega}{c}\boldsymbol{n}\cdot\hat{\mathbf{r}}_j} (\boldsymbol{\xi}\cdot\hat{\mathbf{p}}_j) \middle| \Psi_i \right\rangle, \tag{1.16}$$

where $|\Psi_i\rangle$ is the initial bound state of the molecule and $\langle\Psi_{f,\boldsymbol{k}_f}^{(-)}|$ is the final state with one electron in the continuum with momentum $\boldsymbol{k}_f$ and the residual molecule in state f. Now we apply the dipole approximation where we assume that the wavelength of the field:

$$\lambda = \frac{c}{\omega} \tag{1.17}$$

is much larger than the characteristic dimension of the system being ionized and write:

$$e^{+\mathrm{i}\frac{\omega}{c}\boldsymbol{n}\cdot\hat{\mathbf{r}}_j} = 1 + \sum_{k=1}^{\infty} \frac{1}{k!} \left(\mathrm{i}\frac{\omega}{c}\boldsymbol{n}\cdot\hat{\mathbf{r}}_j \right)^k \approx 1. \tag{1.18}$$

Therefore, in the first order perturbation theory the photoionization amplitude (1.16) reduces to:

$$a_{fi}^{\boldsymbol{\xi}}(\boldsymbol{k}_f) \propto \left\langle \Psi_{f,\boldsymbol{k}_f}^{(-)} \middle| q\boldsymbol{\xi}\cdot\sum_{j=1}^{N} \hat{\mathbf{p}}_j \middle| \Psi_i \right\rangle. \tag{1.19}$$

Using the relation:

$$\hat{\mathbf{p}}_j = -\mathrm{i}\left[\hat{\mathbf{r}}_j, \hat{H}_0\right], \tag{1.20}$$

which is a direct consequence of the commutator between $\hat{\mathbf{r}}$ and $\hat{\mathbf{p}}$, the result (1.19) is rewritten as (Cejnar [2013], p. 156):

$$a_{fi}^{\boldsymbol{\xi}}(\boldsymbol{k}_f) \propto \mathrm{i}(E_{0f} - E_{0i}) \left\langle \Psi_{f,\boldsymbol{k}_f}^{(-)} \middle| \boldsymbol{\xi}\cdot\sum_{j=1}^{N} q\hat{\mathbf{r}}_j \middle| \Psi_i \right\rangle = \mathrm{i}\omega \left\langle \Psi_{f,\boldsymbol{k}_f}^{(-)} \middle| \boldsymbol{\xi}\cdot\sum_{j=1}^{N} q\hat{\mathbf{r}}_j \middle| \Psi_i \right\rangle. \tag{1.21}$$

The operator inside this bracket is the dipole operator:

$$\hat{\mathbf{d}} = \sum_{j=1}^{N} q\hat{\mathbf{r}}_j. \tag{1.22}$$

Since the final ionized state depends on the photoelectron momentum $\boldsymbol{k}_f$, the photoionization amplitude can be written as:

$$a_{fi}^{\boldsymbol{\xi}}(\boldsymbol{k}_f) \propto \mathrm{i}\omega \langle \Psi_{f,\boldsymbol{k}_f}^{(-)} | \boldsymbol{\xi}\cdot\hat{\mathbf{d}} | \Psi_i \rangle = \mathrm{i}\omega\boldsymbol{\xi}\cdot\mathbf{d}_{fi}(\boldsymbol{k}_f), \tag{1.23}$$

where $\mathbf{d}_{fi}(\boldsymbol{k}_f)$ is the dipole matrix element between the initial and the final state which inherits the dependence on the photoelectron momentum from the final state.

[2]The summation index is changed from i to j here in order for it not to be confused with the index of the initial state i.

The photoionization cross section is calculated as the ratio of absorption probability per unit time multiplied by the density of continuum states and the current density of the incoming photons which leads to (Friedrich [2006], p. 131, 135):

$$\sigma = 4\pi^2 \alpha\omega \left|\boldsymbol{\xi}\cdot \mathbf{d}_{fi}(\boldsymbol{k}_f)\right|^2, \tag{1.24}$$

where α is the fine structure constant. In the following, we will identify the photoionization amplitude only with the quantity entering the modulus squared:

$$a^{\boldsymbol{\xi}}_{fi}(\boldsymbol{k}_f) = \boldsymbol{\xi}\cdot \mathbf{d}_{fi}(\boldsymbol{k}_f). \tag{1.25}$$

1.2.2 Partial wave dipoles

The partial wave expansion is a method often used to solve problems of scattering. In case of scattering from a combination of a Coulomb potential and a short-range potential the asymptotic wave function for $r \to \infty$ is given by a sum of Coulomb-corrected plane wave and a modulated outgoing spherical wave (Friedrich [2006], p. 268-269). A slightly modified approach can be used to describe photoionization.

The electron released into the continuum leaves behind a positively charged ion which acts on it with the Coulomb force. Therefore the asymptotic form of the ionized wave function $\Psi^{(-)}_{f,\boldsymbol{k}'_f}(\boldsymbol{r})$ can be written in a very similar way as in case of scattering, only replacing the outgoing spherical wave by the incoming one:

$$\begin{aligned}\Psi^{(-)}_{f,\boldsymbol{k}_f}(\boldsymbol{r}) \quad \xrightarrow[\boldsymbol{r}\to\infty]{} \quad & \frac{1}{(2\pi)^{3/2}}\Bigg[e^{\mathrm{i}\boldsymbol{k}_f\cdot\boldsymbol{r}+\eta\ln[k_f r(1-\hat{\boldsymbol{k}_f}\cdot\hat{\boldsymbol{r}})]} + \\ & +(f_C(\theta)+f(\theta,\varphi))\frac{e^{-\mathrm{i}[k_f r-\eta\ln(2k_f r)]}}{r}\Bigg],\end{aligned} \tag{1.26}$$

where $\boldsymbol{r}$, θ, φ are the spherical coordinates, $\hat{\boldsymbol{k}_f}$ and $\hat{\boldsymbol{r}}$ are the unit vectors in the directions of $\boldsymbol{k}_f$ and $\boldsymbol{r}$, $f_C(\theta)$ is the Coulomb scattering amplitude and $f(\theta,\varphi)$ is the amplitude originating in the short-range part of the interaction. The photoelectron wave function can be expanded into partial waves:

$$\begin{aligned}\Psi^{(-)}_{f,\boldsymbol{k}_f}(\boldsymbol{r}) &= \sum_{l=0}^{\infty}\sum_{m=-l}^{+l} \mathrm{i}^l e^{-\mathrm{i}\sigma_l} Y^*_{lm}(\boldsymbol{k}_f)\Psi^{(-)}_{f,\boldsymbol{k}_f,lm}(\boldsymbol{r}) = \\ &= \sum_{l=0}^{\infty}\sum_{m=-l}^{+l} \mathrm{i}^l e^{-\mathrm{i}\sigma_l} Y^*_{lm}(\boldsymbol{k}_f) R^{(-)}_{lm}(r) Y_{lm}(\boldsymbol{r}),\end{aligned} \tag{1.27}$$

where $R^{(-)}_{lm}(r)$ form the radial part and the spherical harmonics $Y_{lm}(\boldsymbol{r})$ form the angular part of the wave functions and σ_l is the Coulomb phase, see Friedrich [2006], section 1.3.2:

$$\sigma_l = \arg[\Gamma(l+1+i\eta)], \tag{1.28}$$

$$\eta = -\frac{1}{k_f}. \tag{1.29}$$

The sum over the m indices must be present since we consider a general non-spherical interaction. Substituting this partial wave expansion into the relation for the dipole matrix elements (1.23) yields:

$$\boldsymbol{\xi}\cdot \mathbf{d}_{fi}(\boldsymbol{k}_f) = \sum_{lm}(-\mathrm{i})^l e^{\mathrm{i}\sigma_l} Y_{lm}(\boldsymbol{k}_f)\boldsymbol{\xi}\cdot \mathbf{d}_{fi,lm}(k_f), \tag{1.30}$$

where Y_{lm} are the spherical harmonics and $\mathbf{d}_{lm}(k_f)$ are the partial wave dipole matrix elements between the initial state wave function and the partial waves of the final wave function:

$$\mathbf{d}_{fi,lm} = \langle \Psi^{(-)}_{f,\boldsymbol{k}_f,lm} | \hat{\mathbf{d}} | \Psi_i \rangle \tag{1.31}$$

The phase factor in eq. (1.30) is complex conjugated because the final state appears in BRA of the matrix elements (1.31). The use of vectors in the arguments of the spherical harmonics is a simplified notation meaning that the spherical harmonic depends only on the direction of the vector. For example $Y_{lm}(\boldsymbol{k}_f) = Y_{lm}(\theta_{k_f}, \varphi_{k_f})$, where θ_{k_f} and φ_{k_f} are defined by

$$\begin{aligned} k_{fx} &= k_f \sin\theta_{k_f} \cos\varphi_{k_f}, \\ k_{fy} &= k_f \sin\theta_{k_f} \sin\varphi_{k_f}, \\ k_{fz} &= k_f \cos\theta_{k_f}. \end{aligned} \tag{1.32}$$

This notation is used throughout the entire thesis.

The advantage of the partial wave dipole matrix elements $d_{fi,lm}(k_f)$ is that they depend only on the magnitude of the photoelectron momentum, because the dependence on its direction is described by the spherical harmonics in the expansion (1.30). This finds its use in the averaging of the photoelectron angular distribution over all orientations of the molecule which is performed bellow.

1.2.3 Transformation from the lab frame to the molecular frame

To distinguish between the molecular frame and the lab frame the quantities in the lab frame will be denoted as primed.

We consider a photoionization experiment using a laser with a fixed linear polarization and electron detectors at fixed positions in the lab. In this case, the unit photon polarization vector $\boldsymbol{\xi}'$ and the photoelectron momentum $\boldsymbol{k}'_f$ are fixed column vectors in the lab frame.

However, the dipole matrix elements are calculated in the molecular frame. Therefore, the coordinates of the photon polarization and photoelectron momentum vectors have to be transformed into that frame. That is done simply by describing the rotation of the molecule as a rotation $R(\alpha, \beta, \gamma)$ of the molecular frame in the lab parametrized by three Euler angles α, β, γ. The initial orientation of the molecular frame is identified with the lab frame. First the frame rotates around the lab-frame z'-axis by the angle α, then around the new temporary y''-axis by the angle β and finally around the final z-axis by the angle γ ($z' - y'' - z$ convention, explained e.g. in Varshalovich et al. [1988], section 1.4.1, or Brink and Satchler [1968], p. 20 or Cejnar [2013], p. 129), ending up with a rotated molecular frame. The process equivalent to this is firstly rotating the coordinate frame around the original lab-frame z'-axis by the angle γ, then rotating it around the original y'-axis by the angle β and finally around the original z'-axis by the angle α ($z' - y' - z'$ convention). In this second way, all the Euler angles are defined with respect to the initial coordinate system (the lab). Therefore, the 3x3 rotation matrix $R(\alpha, \beta, \gamma)$ is known explicitly, as it is written

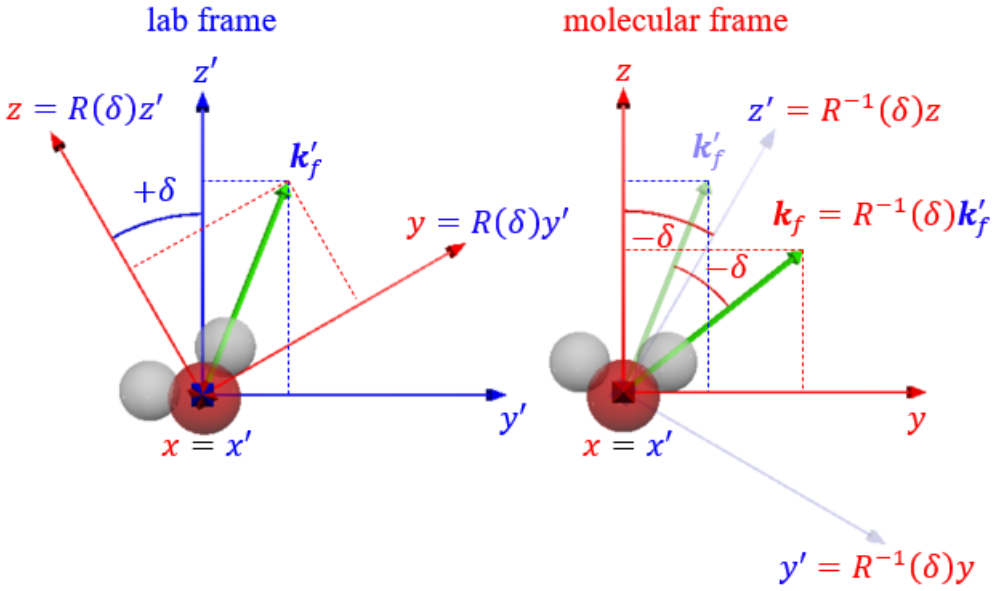

Figure 1.1: Illustration of the meaning of passive and active rotation in the yz plane. Lab frame is blue, molecular frame is red, vector $\boldsymbol{k}'_f$ fixed in the lab frame is green. The basis vectors have the corresponding colors. The color of the symbols of the vector and of the equalities (=) matches the color of the frame in which they are defined. Passive rotation (left): the view from the lab-frame. The mol-frame rotates from its initial position (which is identified with the lab frame) by an angle $+\delta$. The lab-frame and the vector $\boldsymbol{k}'_f$ stay fixed. Active rotation (right): the view from the mol-frame. The mol-frame stays fixed. The vector $\boldsymbol{k}'_f$ rotates from its initial position by an angle $-\delta$, which transforms it to $\boldsymbol{k}_f$.

just as a simple matrix multiplication of these successive rotations:

$$\begin{aligned} R(\alpha,\beta,\gamma) &= A(\alpha)B(\beta)C(\gamma) = \\ &= \begin{pmatrix} \mathrm{c}(\alpha)\mathrm{c}(\beta)\mathrm{c}(\gamma) - \mathrm{s}(\alpha)\mathrm{s}(\gamma) & -\mathrm{c}(\alpha)\mathrm{c}(\beta)\mathrm{s}(\gamma) - \mathrm{s}(\alpha)\mathrm{c}(\gamma) & \mathrm{c}(\alpha)\mathrm{s}(\beta) \\ \mathrm{s}(\alpha)\mathrm{c}(\beta)\mathrm{c}(\gamma) + \mathrm{c}(\alpha)\mathrm{s}(\gamma) & -\mathrm{s}(\alpha)\mathrm{c}(\beta)\mathrm{s}(\gamma) + \mathrm{c}(\alpha)\mathrm{c}(\gamma) & \mathrm{s}(\alpha)\mathrm{s}(\beta) \\ -\mathrm{s}(\beta)\mathrm{c}(\gamma) & \mathrm{s}(\beta)\mathrm{s}(\gamma) & \mathrm{c}(\beta) \end{pmatrix}, \end{aligned} \tag{1.33}$$

where the matrices $A(\alpha)$, $B(\beta)$, $C(\gamma)$ represent the elementary rotations around the axes z', y' and z'. A shortened notation for the trigonometric functions is used: $\mathrm{c}(x) = \cos x$, $\mathrm{s}(x) = \sin x$. The form of the rotational matrix in eq. (1.33) is the same as in Varshalovich et al. [1988], p. 30, and it corresponds to the fact that $R(\alpha,\beta,\gamma)$ is a rotation of the coordinate frame, i.e. a passive rotation (see Man [2017]).

Throughout this entire thesis, we use the same conventions of rotations and rotational operators as Varshalovich et al. [1988] and Brink and Satchler [1968]. The only difference, that must be pointed out, is that in these books the primed coordinate frame is the rotated one, while in this thesis the primed values belong to the lab frame, i.e. the initial (not-rotated) coordinate frame. This is the standard notation used in the atomic and molecular community. Using these

conventions, the rotation of the molecular frame is:

$$\begin{aligned} \boldsymbol{x} &= R(\alpha,\beta,\gamma)\boldsymbol{x}', \\ \boldsymbol{y} &= R(\alpha,\beta,\gamma)\boldsymbol{y}', \\ \boldsymbol{z} &= R(\alpha,\beta,\gamma)\boldsymbol{z}'. \end{aligned} \tag{1.34}$$

These equations express the rotated molecular frame basis vectors $\boldsymbol{x}$, $\boldsymbol{y}$, $\boldsymbol{z}$ in the lab frame.

Since a rotation of the molecular frame in one direction is equivalent to the rotation of the vectors in that frame in the opposite direction (see Man [2017] and figures 1.1 and 1.2), the coordinates of the lab-frame vectors in the rotated molecular frame are obtained by the inverse rotation $R(\alpha,\beta,\gamma)^{-1}$ (see Varshalovich et al. [1988], p. 28-31). Here we apply this to to the vectors of photon polarization and electron momentum:

$$\boldsymbol{\xi} = R(\alpha,\beta,\gamma)^{-1}\boldsymbol{\xi}' = R(-\gamma,-\beta,-\alpha)\boldsymbol{\xi}', \tag{1.35}$$

$$\boldsymbol{k}_f = R(\alpha,\beta,\gamma)^{-1}\boldsymbol{k}'_f = R(-\gamma,-\beta,-\alpha)\boldsymbol{k}'_f. \tag{1.36}$$

Note the opposite order of application of the individual angles in the second equalities. These equations are written in the molecular frame, and vice versa, the inverse transformations $\boldsymbol{k}'_f = R\boldsymbol{k}_f$, $\boldsymbol{\xi}' = R\boldsymbol{\xi}$ are written in the lab frame (see figure 1.2).

Using the relations (1.34)-(1.36) the lab-frame dipole matrix element for an oriented molecule is written as:

$$a_{fi}^{\boldsymbol{\xi}'}(\boldsymbol{k}'_f) = \boldsymbol{\xi}'\cdot\mathbf{d}'_{fi}(\boldsymbol{k}'_f,R) = \boldsymbol{\xi}\cdot\mathbf{d}_{fi}(\boldsymbol{k}_f) = \tag{1.37}$$

$$= (R^{-1}\boldsymbol{\xi}')\cdot\mathbf{d}_{fi}(R^{-1}\boldsymbol{k}'_f). \tag{1.38}$$

1.2.4 Averaging over all orientations of the molecule

To calculate the angular distribution (the differential cross section) of photoelectrons released from a gas of randomly oriented molecules, the transition probability must be averaged over all possible orientations of the molecule in the lab frame, i.e. integrated over all possible rotations of the molecular frame:

$$\begin{aligned} \left(\frac{\mathrm{d}\sigma}{\mathrm{d}\boldsymbol{k}'_f}\right)_{Av} &= 4\pi^2\alpha\omega\frac{1}{8\pi^2}\int \mathrm{d}R\left|a_{fi}^{\boldsymbol{\xi}'}(\boldsymbol{k}'_f)\right|^2 = \\ &= 4\pi^2\alpha\omega\frac{1}{8\pi^2}\int \mathrm{d}R\left|\boldsymbol{\xi}'\cdot\mathbf{d}'_{fi}(\boldsymbol{k}'_f,R)\right|^2, \end{aligned} \tag{1.39}$$

where for simplicity $\int \mathrm{d}R$ denotes: $\int \mathrm{d}R = \int_0^{2\pi}\mathrm{d}\alpha\int_0^{\pi}\sin(\beta)\mathrm{d}\beta\int_0^{2\pi}\mathrm{d}\gamma$. That can be done either analytically or numerically. The analytic approach, using the partial wave expansion of the dipoles and relations for the rotational operators will be developed here in this subsection. The numerical approach, using adaptive Gauss-Legendre quadrature, will be described in Chapter 2. For a single molecule the numerical calculations were used primarily to verify the correctness of the analytic results.

For simplicity in the following the photon polarization will be set either to linear or left- or right-handed circular. To describe the photon polarization we

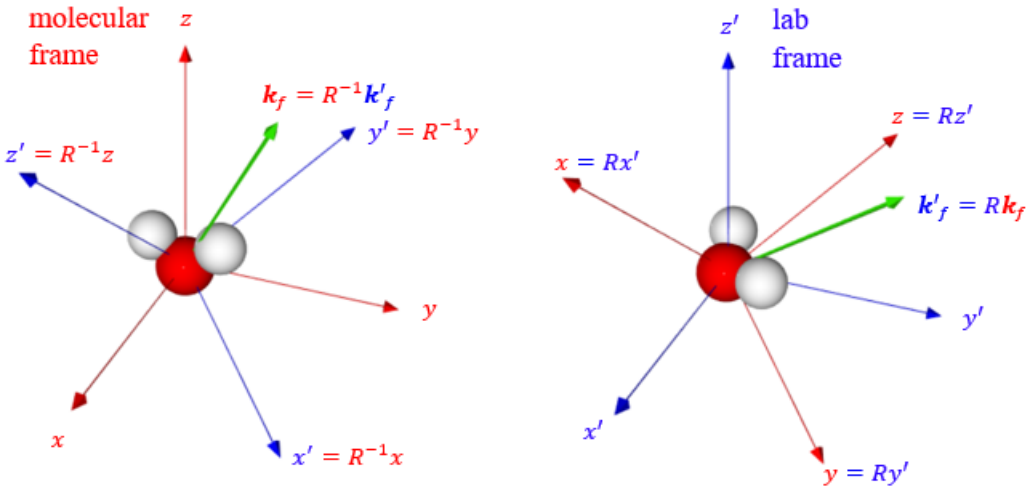

Figure 1.2: Illustration of the rotation of the molecular frame $R(\alpha, \beta, \gamma)$, its inverse $R^{-1}(\alpha, \beta, \gamma) = R(-\gamma, -\beta, -\alpha)$ and the corresponding vector transformations in 3D. The molecular frame is red, the lab frame is blue. Their basis vectors have the corresponding colors. The photoelectron momentum vector $\boldsymbol{k}'_f$ is depicted as the green arrow in both frames and is fixed in the lab frame. The color of the symbols of the vector and of the equalities (=) matches the color of the frame in which they are defined.

take advantage of using the so called covariant spherical coordinates x_p, where $p \in \{-1, 0, +1\}$, defined via their relations to the Cartesian and spherical coordinates as (see Varshalovich et al. [1988], p. 5):

$$\begin{aligned} x_{+1} &= -\frac{1}{\sqrt{2}}(x + \mathrm{i}y) = -\frac{1}{\sqrt{2}} r \sin\theta e^{\mathrm{i}\varphi}, \\ x_0 &= z = r\cos\theta, \\ x_{-1} &= \frac{1}{\sqrt{2}}(x + \mathrm{i}y) = \frac{1}{\sqrt{2}} r \sin\theta e^{-\mathrm{i}\varphi}, \end{aligned} \tag{1.40}$$

where r, θ and φ are the spherical coordinates defined by:

$$\begin{aligned} x &= r\sin\theta\cos\varphi, \\ y &= r\sin\theta\sin\varphi, \\ z &= r\cos\theta, \end{aligned} \tag{1.41}$$

where θ is the polar angle and φ is the azimuthal angle. For linearly polarized light, the z-axis is identified with the direction of the polarization, while for circularly polarized light, the z-axis is identified with the direction of the photon propagation with the electric field vector rotating in the xy plane. Hence, in this covariant spherical basis, the linear photon polarization corresponds to $p = 0$ and circular polarization corresponds to $p = \pm 1$ (left or right circular polarization).

Therefore, when only one of these three special cases of the photon polarization is chosen, the unit polarization vector $\boldsymbol{\xi}'$ will have only one non-zero component (e.g. polarization along the z'-axis corresponds to $p = 0$), which reduces the relation (1.37) so that we can write:

$$a^p_{fi}(\boldsymbol{k}'_f) = d'^p_{fi}(\boldsymbol{k}'_f, R), \tag{1.42}$$

where again, as before, the primed quantities and vectors are defined in the lab-frame.

However, using directly the lab-frame dipoles to perform the rotational averaging would require a separate calculation of the dipoles for each rotation R of the molecule. This direct approach makes the analytic averaging impossible. Instead, we can express the lab-frame dipoles using the dipoles calculated in the molecular frame in the partial wave basis and then apply the well-known properties of spherical harmonics under rotations.

The expression of the lab-frame dipole in the partial-wave basis with respect to the lab coordinate frame is:

$$d'^{p}_{fi}(\boldsymbol{k}'_f, R) = \sum_{lm} (-\mathrm{i})^l e^{\mathrm{i}\sigma_l} Y'_{lm}(\boldsymbol{k}'_f) d'^{p}_{lm}(k'_f), \tag{1.43}$$

where for clarity Y'_{lm} denote explicitly spherical harmonics in the lab-frame basis. However, Y'_{lm} and Y_{lm} are obviously the same functions, hence we drop the prime from now on. Just as d'^{p}_{fi} in eq. (1.42), the partial wave dipoles d'^{p}_{lm} in the relation (1.43) are still in the lab-frame and depend only on the magnitude of the photoelectron momentum $k'_f = k_f$, which does not change by rotation. They are defined as the matrix elements of the dipole operator:

$$d'^{p}_{fi,lm} = \langle \Psi'^{(-)}_{f,\boldsymbol{k}_f,lm} | \hat{\mu}_p | \Psi'_i \rangle, \tag{1.44}$$

where

$$\hat{\mu}_p = \sqrt{\frac{4\pi}{3}} r Y_{1p} \tag{1.45}$$

and $\Psi'^{(-)}_{f,\boldsymbol{k}_f,lm}(\mathbf{r}')$ is the partial wave component of the wave function. The dipole matrix elements in the molecular frame are, of course, defined in the very same way, only without the primes:

$$d^{p}_{fi,lm} = \sqrt{\frac{4\pi}{3}} r \langle \Psi^{(-)}_{f,\boldsymbol{k}_f,lm} | Y_{1p} | \Psi_i \rangle. \tag{1.46}$$

The indices fi in $d'^{p}_{fi,lm}$ and $d^{p}_{fi,lm}$ are still those of the initial $|\Psi_i\rangle$ and final $|\Psi^{(-)}_{f,\boldsymbol{k}_f}\rangle$ states. Since these states are considered fixed, the indices fi will be omitted from now on.

In order to establish connection between the dipoles in the two frames of reference the lab-frame spherical harmonics $Y_{1p}(\mathbf{r}')$ of the photon and $Y_{lm}(\mathbf{r}')$ of the photoelectron have to be expressed in terms of the molecular-frame spherical harmonics $Y_{1p}(\mathbf{r})$ and $Y_{lm}(\mathbf{r})$ and the lab-frame initial and final states have to be replaced with those from the molecular frame. That is accomplished utilizing the Wigner rotation matrices.

Since, as was already written above, rotation R is defined as the rotation from the lab frame to the molecular frame (see eq. (1.34)), the angular momentum basis in the rotated mol-frame is obtained applying a unitary operator (as it represents a rotation) on the angular basis in the lab-frame (see Brink and Satchler [1968],

p. 27-28, or Varshalovich et al. [1988], p. 27)[3]:

$$|lm\rangle = D(R)|lm\rangle' = \sum_{\mu} {}'\langle l\mu|D(R)|lm\rangle'|l\mu\rangle' = \sum_{\mu} D^{l}_{\mu,m}(R)|l\mu\rangle', \quad (1.47)$$

$$\langle \mathbf{r}|lm\rangle = Y_{lm}(\mathbf{r}) = \sum_{\mu} D^{l}_{\mu,m}(R) Y_{l\mu}(\mathbf{r}'), \quad (1.48)$$

where $D^{l}_{\mu,m}(R)$ are the Wigner rotation matrices. Therefore, the bra of the photoelectron wave function that enters into eq (1.43) can be expressed using the inverse of the transformation (1.48) as:

$$\langle \Psi'^{(-)}_{lm}|\mathbf{r}'\rangle = \left[R^{(-)}_{lm}(r)\right]^{*} Y^{*}_{lm}(\mathbf{r}') = \left[R^{(-)}_{lm}(r)\right]^{*} \left[\sum_{\mu} D^{l}_{\mu,m}(R^{-1}) Y_{l\mu}(\mathbf{r})\right]^{*}. \quad (1.49)$$

The lab-frame spherical harmonic of the photon is written similarly, as the inverse of the transformation (1.48):

$$Y_{1p}(\mathbf{r}') = \sum_{q} D^{1}_{q,p}(R^{-1}) Y_{1q}(\mathbf{r}). \quad (1.50)$$

Thus, substituting equations (1.49) and (1.50) into (1.44) and finally into (1.43) while simultaneously removing primes from the initial and final photoelectron wave functions gives the relation for the lab-frame dipole amplitude in terms of quantities calculated in the molecular frame:

$$d'^{p}_{fi}(\boldsymbol{k}'_f, R) = \sum_{lm} (-\mathrm{i})^{l} e^{\mathrm{i}\sigma_l} Y_{lm}(\boldsymbol{k}'_f) \sum_{\mu,q} \left[D^{l}_{\mu,m}(R^{-1})\right]^{*} D^{1}_{q,p}(R^{-1}) d^{q}_{l\mu}(k_f). \quad (1.51)$$

Using the relations for the rotational matrices:

$$\left[D^{l}_{\mu,m}(R^{-1})\right]^{*} = D^{l}_{m,\mu}(R), \quad (1.52)$$

$$D^{1}_{q,p}(R^{-1}) = \left[D^{1}_{p,q}(R)\right]^{*}, \quad (1.53)$$

which are consequences of the properties of the unitary character of the rotation R, we further simplify the equation (1.51):

$$d'^{p}_{fi}(\boldsymbol{k}'_f, R) = \sum_{lm} (-\mathrm{i})^{l} e^{\mathrm{i}\sigma_l} Y_{lm}(\boldsymbol{k}'_f) \sum_{\mu,q} D^{l}_{m,\mu}(R) \left[D^{1}_{p,q}(R)\right]^{*} d^{q}_{l\mu}(k_f). \quad (1.54)$$

Swapping the notation for m and μ and rearranging the sums gives the relation:

$$d'^{p}_{fi}(\boldsymbol{k}'_f, R) = \sum_{lm} (-\mathrm{i})^{l} e^{\mathrm{i}\sigma_l} \sum_{\mu} Y_{l\mu}(\boldsymbol{k}'_f) D^{l}_{\mu,m}(R) \sum_{q} \left[D^{1}_{p,q}(R)\right]^{*} d^{q}_{lm}(k_f). \quad (1.55)$$

For simplicity, from now on we absorb the phase factors $(-\mathrm{i})^{l} e^{\mathrm{i}\sigma_l}$ into the dipole matrix element:

$$(-\mathrm{i})^{l} e^{\mathrm{i}\sigma_l} d^{q}_{lm} \to d^{q}_{lm}. \quad (1.56)$$

Finally, the relation for the lab-frame dipole amplitudes can be written as:

$$d'^{p}_{fi}(\boldsymbol{k}'_f, R) = \sum_{lm} \sum_{\mu} Y_{l\mu}(\boldsymbol{k}'_f) D^{l}_{\mu,m}(R) \sum_{q} \left[D^{1}_{p,q}(R)\right]^{*} d^{q}_{lm}(k_f). \quad (1.57)$$

[3]Remember that the definition of primed and unprimed systems in Varshalovich et al. [1988] is opposite to that in this thesis.

With that, we can now move to the analytical averaging over all orientations of the molecule. Substituting eq. (1.57) into the integral $\int \mathrm{d}R$ in eq. (1.39) yields:

$$\left(\frac{\mathrm{d}\sigma}{\mathrm{d}\boldsymbol{k}'_f}\right)_{Av} = 4\pi^2\alpha\omega\frac{1}{8\pi^2}\int \mathrm{d}R d^{p\,\prime}_{fi}(\boldsymbol{k}'_f,R)\left[d^{p\,\prime}_{fi}(\boldsymbol{k}'_f,R)\right]^* = \tag{1.58}$$

$$= \frac{4\pi^2\alpha\omega}{8\pi^2}\int \mathrm{d}R\left|\sum_{lm}\sum_{\mu} Y_{l\mu}(\boldsymbol{k}'_f)D^l_{\mu,m}(R)\sum_q\left[D^1_{p,q}(R)\right]^* d^q_{lm}(k_f)\right|^2 = \tag{1.59}$$

$$= \frac{\alpha\omega}{2}Y_{l\mu}(\boldsymbol{k}'_f)Y^*_{l'\mu'}(\boldsymbol{k}'_f)\int \mathrm{d}R\sum_{lm}\sum_{l'm'}\sum_{\mu}\sum_{\mu'}\sum_{q}\sum_{q'}\times$$

$$\times D^l_{\mu,m}(R)\left[D^{l'}_{\mu',m'}(R)\right]^*\left[D^1_{p,q}(R)\right]^* D^1_{p,q'}(R)d^q_{lm}(k_f)\left[d^{q'}_{l'm'}(k_f)\right]^*. \tag{1.60}$$

In the following, the relation (1.60) will be simplified using the relations for the Wigner D-matrices (Brink and Satchler [1968]) in order to rewrite it into the shape of the general formula (1.5).

Firstly, we can couple, separately, the photon and electron angular momenta:

$$\left[D^1_{p,q}(R)\right]^* D^1_{p,q'}(R) = (-1)^{p-q}D^1_{-p,-q}(R)D^1_{p,q'}(R) =$$

$$= (-1)^{p-q}\sum_K(2K+1)\begin{pmatrix}1 & 1 & K\\ -p & p & 0\end{pmatrix}\begin{pmatrix}1 & 1 & K\\ -q & q' & M_K\end{pmatrix}\left[D^K_{0,M_K}\right]^*, \tag{1.61}$$

$$\left[D^{l'}_{\mu',m'}(R)\right]^* D^l_{\mu,m}(R) = (-1)^{\mu'-m'}D^l_{\mu,m}(R)D^{l'}_{-\mu',-m'}(R) =$$

$$= (-1)^{\mu'-m'}\sum_\lambda(2\lambda+1)\begin{pmatrix}l & l' & \lambda\\ \mu & -\mu' & M_\lambda\end{pmatrix}\begin{pmatrix}l & l' & \lambda\\ m & -m' & M_{\lambda'}\end{pmatrix}\times$$

$$\times\left[D^\lambda_{M_\lambda,M_{\lambda'}}\right]^*, \tag{1.62}$$

where $\begin{pmatrix}l & l' & L\\ m & m' & M\end{pmatrix}$ are the Wigner 3-j symbols and the index M is fixed by the selection rule (Varshalovich et al. [1988], p. 235-236):

$$m + m' + M = 0. \tag{1.63}$$

The orthogonality relation between Wigner D-matrices can now be used to perform the integral over R:

$$\int \mathrm{d}R\left[D^\lambda_{M_\lambda,M_{\lambda'}}\right]^*\left[D^K_{0,M_K}\right]^* = \int \mathrm{d}R\left[D^\lambda_{M_\lambda,M_{\lambda'}}\right]^* D^K_{0,-M_K}(-1)^{-M_K} =$$

$$= \delta_{\lambda,K}\delta_{M_\lambda,0}\delta_{M_{\lambda'},-M_K}(-1)^{-M_K}\frac{8\pi^2}{2K+1}. \tag{1.64}$$

This result implies constraints on some of the indices:

$$\begin{aligned}\lambda &= K,\\ \mu' &= \mu,\\ m'-m &= q'-q,\end{aligned} \tag{1.65}$$

and the selection rules for the angular momenta in the 3-j symbols (Varshalovich et al. [1988], p. 235-236) yield:

$$\begin{aligned}K &\leq 2,\\ \lambda &\leq 2.\end{aligned} \tag{1.66}$$

We contract the spherical harmonics of the photoelectron momentum keeping for a moment the index μ' as it is (see Brink and Satchler [1968], Appendix IV):

$$\begin{aligned} Y_{l\mu}(\boldsymbol{k}'_f)Y^*_{l'\mu'}(\boldsymbol{k}'_f) &= \sum_{L,M}(-1)^{\mu'}\sqrt{\frac{(2l+1)(2l'+1)(2L+1)}{4\pi}}\times \\ &\times \begin{pmatrix} l & l' & L \\ 0 & 0 & 0 \end{pmatrix}\begin{pmatrix} l & l' & L \\ \mu & -\mu' & M \end{pmatrix} Y^*_{LM}(\boldsymbol{k}'_f), \end{aligned} \tag{1.67}$$

which makes it possible to apply one of the orthogonality relations between the Wigner 3-j symbols (see Brink and Satchler [1968], Appendix I) to one 3-j symbol from eq. (1.62) and one from eq (1.67):

$$\sum_{\mu,\mu'}(2\lambda+1)\begin{pmatrix} l & l' & \lambda \\ \mu & -\mu' & M_\lambda \end{pmatrix}\begin{pmatrix} l & l' & L \\ \mu & -\mu' & M \end{pmatrix} = \delta_{\lambda,L}\delta_{M_\lambda,M}. \tag{1.68}$$

This implies:

$$\begin{aligned} 0 \le L = \lambda = K \le 2, \\ M_\lambda = M = \mu' - \mu = 0, \end{aligned} \tag{1.69}$$

which means that the photoelectron angular distribution contains only real spherical harmonics with $K \le 2$ and $M = 0$ in agreement with Yang's theorem (1.5).

Inserting all these equations into the formula (1.60), while noticing that the factor $(-1)^{\mu'}$ from the equation (1.67) and the same factor from the relation (1.62) cancel out, gives:

$$\begin{aligned} \left(\frac{\mathrm{d}\sigma}{\mathrm{d}\boldsymbol{k}'_f}\right)_{Av} &= 4\pi^2\alpha\omega\frac{1}{8\pi^2}\sum_K\sum_{l,m}\sum_{l',m'}\sum_{q,q'}(-1)^{p-q}\frac{2K+1}{2K+1}8\pi^2(-1)^{q'-q}(-1)^{-m'} \\ &\times\sqrt{\frac{(2l+1)(2l'+1)(2K+1)}{4\pi}}\begin{pmatrix} l & l' & K \\ m & -m' & m'-m \end{pmatrix}\begin{pmatrix} l & l' & K \\ 0 & 0 & 0 \end{pmatrix} \\ &\times\begin{pmatrix} 1 & 1 & K \\ -p & p & 0 \end{pmatrix}\begin{pmatrix} 1 & 1 & K \\ -q & q' & m-m' \end{pmatrix} d^q_{lm}(k_f)\left[d^{q'}_{l'm'}(k_f)\right]^* Y_{K,0}(\boldsymbol{k}'_f). \end{aligned} \tag{1.70}$$

Simplifying the numerical factors and expressing the spherical harmonics in terms of Legendre polynomials (see e.g. Brink and Satchler [1968], Appendix IV) as:

$$Y_{K0}(\boldsymbol{k}'_f) = \sqrt{\frac{2K+1}{4\pi}}P_K(\cos\theta'), \tag{1.71}$$

where θ' is the angle measured from the lab-frame z' axis, finally leads to the definitive result for orientationally averaged angular distribution of photoelectrons:

$$\begin{aligned} \left(\frac{\mathrm{d}\sigma}{\mathrm{d}\boldsymbol{k}'_f}\right)_{Av} &= \frac{1}{4\pi}4\pi^2\alpha\omega\sum_K\sum_{l,m}\sum_{l',m'}\sum_{q,q'}(-1)^{p+q'-m'}\sqrt{(2l+1)(2l'+1)} \\ &\times(2K+1)\begin{pmatrix} l & l' & K \\ m & -m' & m'-m \end{pmatrix}\begin{pmatrix} l & l' & K \\ 0 & 0 & 0 \end{pmatrix}\begin{pmatrix} 1 & 1 & K \\ -p & p & 0 \end{pmatrix} \\ &\times\begin{pmatrix} 1 & 1 & K \\ -q & q' & m-m' \end{pmatrix} d^q_{lm}(k_f)\left[d^{q'}_{l'm'}(k_f)\right]^* P_K(\cos\theta'). \end{aligned} \tag{1.72}$$

This result can be rewritten compactly as:

$$\left(\frac{\mathrm{d}\sigma}{\mathrm{d}\boldsymbol{k}'_f}\right)_{Av} = \frac{1}{4\pi}\sum_K A_K P_K(\cos\theta'), \tag{1.73}$$

where A_K embraces all the other sums and the pre-factor $4\pi^2\alpha\omega$. Comparison with the standard formula (1.5) immediately gives expressions for the σ, β_1, β_2 parameters:

$$\sigma(E) = A_0, \tag{1.74}$$

$$\beta_1(E) = \frac{A_1}{A_0}, \tag{1.75}$$

$$\beta_2(E) = \frac{A_2}{A_0}. \tag{1.76}$$

This means that each β parameter can be calculated separately by fixing the index K and carrying out the remaining summations in eq. (1.72).

However, since the H_2O molecule has two planes of symmetry, the parameter $\beta_1(E)$ is always zero for a single water molecule (see Ritchie [1976] or the discussion in Section 1.1).

Before moving to molecular clusters, an important property can be proved. If $K = 0$, the selection rules for the 3-j symbols immediately imply:

$$\begin{aligned} l &= l', \\ m = m' &\Rightarrow q = q'. \end{aligned} \tag{1.77}$$

This means that:

$$\sigma(E) = 4\pi^2\alpha\omega\sum_{l,m}(2l+1)\left|d^q_{lm}(k_f)\right|^2, \tag{1.78}$$

i.e. the integral cross section is proportional to the sum of squares of the dipole matrix elements.

1.3 Independent molecule model of cluster photoionization

In this section, the relations for integral cross section and asymmetry parameters of the the angular distribution of photoelectrons released from a single molecule will be generalised to a simplified model of photoionization of water molecular clusters.

The photoionization of a cluster can be described using a modification of the so called independent scattering center approximation (see Massey et al. [1969], section 10.1.1, p. 666-668) which was developed to describe electron scattering from molecules. This model treats the scattering of electrons from molecules as if each atom scattered independently, neglecting the multiple scattering from the other atoms of the molecule and the redistribution of electrons caused by the bonds between the atoms. An independent molecule model (IMM) of photoionization of a molecular cluster based on similar assumptions is formulated bellow.

1.3.1 Photoionization amplitude for a cluster

In this section we derive an approximate expression for the photoionization amplitude for a cluster starting from the amplitude in the lab-frame:

$$a_{fi}^{\boldsymbol{\xi}'}(\boldsymbol{k}'_f) = \langle \Psi'^{(-),c}_{f,\boldsymbol{k}'_f} | \boldsymbol{\xi}' \cdot \hat{\mathbf{d}}' | \Psi'^{c}_{i} \rangle, \tag{1.79}$$

where $|\Psi^c_i\rangle$ is the initial (bound) state of the cluster and $\langle \Psi^{(-),c}_{f,\boldsymbol{k}'_f}|$ is the final continuum state describing the electron outgoing with momentum $\boldsymbol{k}'_f$ and the cluster in a ionic state f. The initial state can be approximated by a direct product of the bound states of the constituent monomers:

$$|\Psi'^{c}_{i}\rangle = |\Psi'_{g,1}\rangle |\Psi'_{g,2}\rangle \ldots |\Psi'_{g,n}\rangle, \tag{1.80}$$

where n is the number of molecules in the cluster. Doing this we neglect the charge redistribution in the cluster and electron exchange between the monomers. Similarly, the final state can be approximated as a coherent superposition of the direct products of monomer states where one of them was ionized:

$$\langle \Psi'^{(-),c}_{f,\boldsymbol{k}'_f}| = \sum_{j=1}^{n} \langle \Psi'_{g,1}| \ldots \langle \Psi'^{(-)}_{f,\boldsymbol{k}'_f,j}| \ldots \langle \Psi'_{g,n}|. \tag{1.81}$$

The form (1.81) additionally neglects the multiple scattering of photoelectrons from the field of the cluster. Substituting the expressions (1.80) and (1.81) into the relation (1.79) yields:

$$a_{fi}^{\boldsymbol{\xi}'}(\boldsymbol{k}'_f) = \langle \Psi'^{(-),c}_{f,\boldsymbol{k}'_f} | \boldsymbol{\xi}' \cdot \hat{\mathbf{d}}' | \Psi'^{c}_{i} \rangle = \sum_{j=1}^{n} \langle \Psi'^{(-)}_{f,\boldsymbol{k}'_f,j} | \boldsymbol{\xi}' \cdot \hat{\mathbf{d}}' | \Psi'_{g,j} \rangle. \tag{1.82}$$

These approximations are the main assumptions of our independent molecule model.

If the electron exchange between the monomers in the initial state was not neglected, the equation (1.82) would also have to include the cross-terms:

$$\langle \Psi'^{(-)}_{f,\boldsymbol{k}'_f,i} | \boldsymbol{\xi}' \cdot \hat{\mathbf{d}} | \Psi'_{g,j} \rangle, i \neq j. \tag{1.83}$$

These terms involve overlap of the photoelectron wave function centered on one molecule with the bound state wave function centered on another molecule. This yields a two-center integral, thus the cross-terms would be more difficult to evaluate.

However, the relation (1.82) is still not the correct representation of the cluster photoionization amplitude. Just as for a single molecule (eq. 1.26), the photoelectron wave function for a cluster is defined by the Coulomb-corrected incoming wave asymptotic boundary conditions (Friedrich [2006], p. 269):

$$\begin{aligned} \Psi'^{(-),c}_{f,\boldsymbol{k}'_f}(\boldsymbol{r}') \quad \xrightarrow[r'\to\infty]{} \quad & \frac{1}{(2\pi)^{3/2}} \Bigg[e^{\mathrm{i}\boldsymbol{k}'_f \cdot \boldsymbol{r}' + \eta \ln[k_f r(1 - \hat{\boldsymbol{k}}'_f \cdot \hat{\boldsymbol{r}}')]} + \\ & + (f_C(\theta') + f(\theta', \varphi')) \frac{e^{-\mathrm{i}[k_f r - \eta \ln(2k_f r)]}}{r} \Bigg], \end{aligned} \tag{1.84}$$

where $\boldsymbol{r}'$ is measured from the cluster center of mass and $\hat{\boldsymbol{k}}'_f$ and $\hat{\boldsymbol{r}}'$ are the unit vectors in the directions of $\boldsymbol{k}'_f$ and $\boldsymbol{r}'$, $f_C(\theta')$ is the Coulomb scattering amplitude and $f(\theta', \varphi')$ is the contribution from the short-range part of the electron-cluster interaction. Clearly, the monomer wave functions which are centered on the centers of mass of the molecules do not satisfy the condition (1.84). Instead, their asymptotic forms are shifted:

$$\Psi'^{(-),c}_{f,\boldsymbol{k}'_f,j}(\boldsymbol{r}') \xrightarrow[r'\to\infty]{} \frac{1}{(2\pi)^{3/2}}\left[e^{\mathrm{i}\boldsymbol{k}'_f\cdot(\boldsymbol{r}'-\boldsymbol{\rho}_j)+\eta\ln[k_f\|\boldsymbol{r}'-\boldsymbol{\rho}'_j\|(1-\hat{\boldsymbol{k}}'_f\cdot(\widehat{\boldsymbol{r}'-\boldsymbol{\rho}'_j}))]} + \right.$$
$$\left. +(f_C(\theta')+f(\theta',\varphi'))\frac{e^{-\mathrm{i}[k_f\|\boldsymbol{r}'-\boldsymbol{\rho}'_j\|-\eta\ln(2k_f\|\boldsymbol{r}'-\boldsymbol{\rho}'_j\|)]}}{r}\right], \quad (1.85)$$

where $\boldsymbol{\rho}'_j$ is the position of the center of mass of j-th molecule of the cluster. Hence, the wave function $\Psi^{(-)}_{f,\boldsymbol{k}'_f,j}(\boldsymbol{r}')$ must be modified to give the proper asymptotic form (1.84) before substituting it into the equation (1.82). In particular, since in the time-dependent formulation only the plane-wave part survives at $t\to\infty$ (i.e. at the time of observation), it must be ensured that the first terms from the equations (1.84) and (1.85), corresponding to the Coulomb-corrected plane wave, are the same.

In order to do that, we neglect the logarithmic correction which is not separable. Therefore, we replace the Coulomb-corrected plane wave with a regular plane wave:

$$e^{\mathrm{i}\boldsymbol{k}'_f\cdot(\boldsymbol{r}'-\boldsymbol{\rho}'_j)+\eta\ln[k_f\|\boldsymbol{r}'-\boldsymbol{\rho}'_j\|(1-\hat{\boldsymbol{k}}'_f\cdot(\widehat{\boldsymbol{r}'-\boldsymbol{\rho}'_j}))]} \sim e^{\mathrm{i}\boldsymbol{k}'_f\cdot(\boldsymbol{r}'-\boldsymbol{\rho}'_j)}. \quad (1.86)$$

Considering that in a real cluster environment the Coulomb potential might be shielded, this approximation is crude but may not be unreasonable. This yields that the monomer wave functions $\Psi^{(-)}_{f,\boldsymbol{k}'_f,j}(\boldsymbol{r}')$, entering the relation (1.82), must be replaced with:

$$e^{\mathrm{i}\boldsymbol{k}'_f\cdot\boldsymbol{\rho}'_j}\Psi'^{(-)}_{f,\boldsymbol{k}'_f,j}(\boldsymbol{r}'). \quad (1.87)$$

The additional phase factor has the interpretation of the phase difference between the electron waves emitted from the different monomers. Thus the final expression for the photoionization amplitude for a cluster in the independent molecule model is:

$$a^{\xi'}_{fi}(\boldsymbol{k}'_f) = \sum_{j=1}^{n} e^{\mathrm{i}\boldsymbol{k}'_f\cdot\boldsymbol{\rho}'_j}\langle\Psi'^{(-)}_{f,\boldsymbol{k}'_f,j}|\boldsymbol{\xi}'\cdot\hat{\mathbf{d}}'|\Psi'_{g,j}\rangle, \quad (1.88)$$

which is a coherent superposition of the amplitudes for the individual molecules of the cluster.

1.3.2 Averaging over all orientations of the cluster

Except for the molecular frame dipole matrix elements, in order to preserve their denotation without primes, from now on, the unprimed values will be written in the cluster frame. If it is needed to write a value in a molecular frame of a certain molecule of the cluster, it will be indicated by a superscript MFj, meaning molecular frame of the j-th molecule.

Starting from the relation (1.88) we can write the expression for the photoelectron angular distribution of the cluster in our IMM model as:

$$\left(\frac{\mathrm{d}\sigma}{\mathrm{d}\boldsymbol{k}'_f}\right)_{Av} = 4\pi^2\alpha\omega\frac{1}{8\pi^2}\int \mathrm{d}R_{CF}\left|\sum_{j=1}^{n} e^{\mathrm{i}(\boldsymbol{k}'_f\cdot\boldsymbol{\rho}'_j)} d'^{p}_{fi}(\boldsymbol{k}'_f, R_j)\right|^2, \tag{1.89}$$

where n is the number of molecules in the $(H_2O)_n$ cluster, R_j is the orientation of j-th molecule with respect to the lab frame (the rotation of the j-th molecular frame from the lab frame), R_{CF} is the orientation of the entire cluster with respect to the lab frame (the rotation of the cluster frame from the lab frame), $d'^{p}_{fi}(\boldsymbol{k}'_f, R_j)$ is the lab-frame dipole of j-th molecule. This means, that one dipole element for a single molecule is just replaced by a coherent superposition of the dipole elements of all molecules in the cluster.

Now we need to deal with the rotations R_j. In our model, the cluster rotates in the lab frame as a single solid body, with molecules fixed in it. Hence, the orientation of each molecule with respect to the lab frame R_j can be written as a composition of a rotation of the cluster frame in the lab (R_{CF}) and a rotation (orientation) of the particular molecular frame in the cluster ($\tilde{R}_{MFj}$):

$$R_j(\alpha,\beta,\gamma) = \tilde{R}_{MFj}(\alpha_{MFj},\beta_{MFj},\gamma_{MFj})R_{CF}(\alpha_{CF},\beta_{CF},\gamma_{CF}), \tag{1.90}$$

where the tilde in $\tilde{R}_{MFj}(\alpha_{MFj},\beta_{MFj},\gamma_{MFj})$ denotes, that $\tilde{R}_{MFj}$ (and its Euler angles) of each molecule is defined with respect to the cluster frame (not the lab frame, see fig. 1.3). This is important, because it actually enables the integration over R_{CF} to be performed independently from $\tilde{R}_{MFj}$. However, the angles $\alpha_{CF},\beta_{CF},\gamma_{CF}$ of the rotation of the cluster are defined with respect to the lab frame. This means that the operator of the second rotation $\tilde{R}_{MFj}$ must be transformed from the intermediate cluster frame basis into the lab frame basis (see Varshalovich et al. [1988], section 1.4.7). That is done by the operator transformation:

$$\tilde{R}_{MFj} = R_{CF}R_{MFj}R_{CF}^{-1}. \tag{1.91}$$

Therefore, the rotations in (1.90) actually swap the order after rewriting both into the same basis:

$$R_j = R_{CF}R_{MFj}R_{CF}^{-1}R_{CF} = R_{CF}R_{MFj} \tag{1.92}$$

The order of the rotations is crucial since in 3D the rotations generally do not commute. Note, that this is actually the same principle swapping the elementary rotations by the Euler angles α and γ from the $z'-y''-z$ form to the $z'-y'-z'$ form (see e.g. Cejnar [2013], p. 129 and the discussion above eq. 1.33).

Hence, with the relation (1.90) the rotations of the photon polarization vector and the photoelectron momentum vector from the lab frame into the j-th molecular frame can be written as:

$$\boldsymbol{\xi}^{MFj} = R_j^{-1}\boldsymbol{\xi}' = R_{MFj}^{-1}R_{CF}^{-1}\boldsymbol{\xi}', \tag{1.93}$$

$$\boldsymbol{k}_f^{MFj} = R_j^{-1}\boldsymbol{k}'_f = R_{MFj}^{-1}R_{CF}^{-1}\boldsymbol{k}'_f \tag{1.94}$$

With the relations (1.89) and (1.92), the formula for the orientationally averaged differential cross section for a cluster can be derived in a similar way as

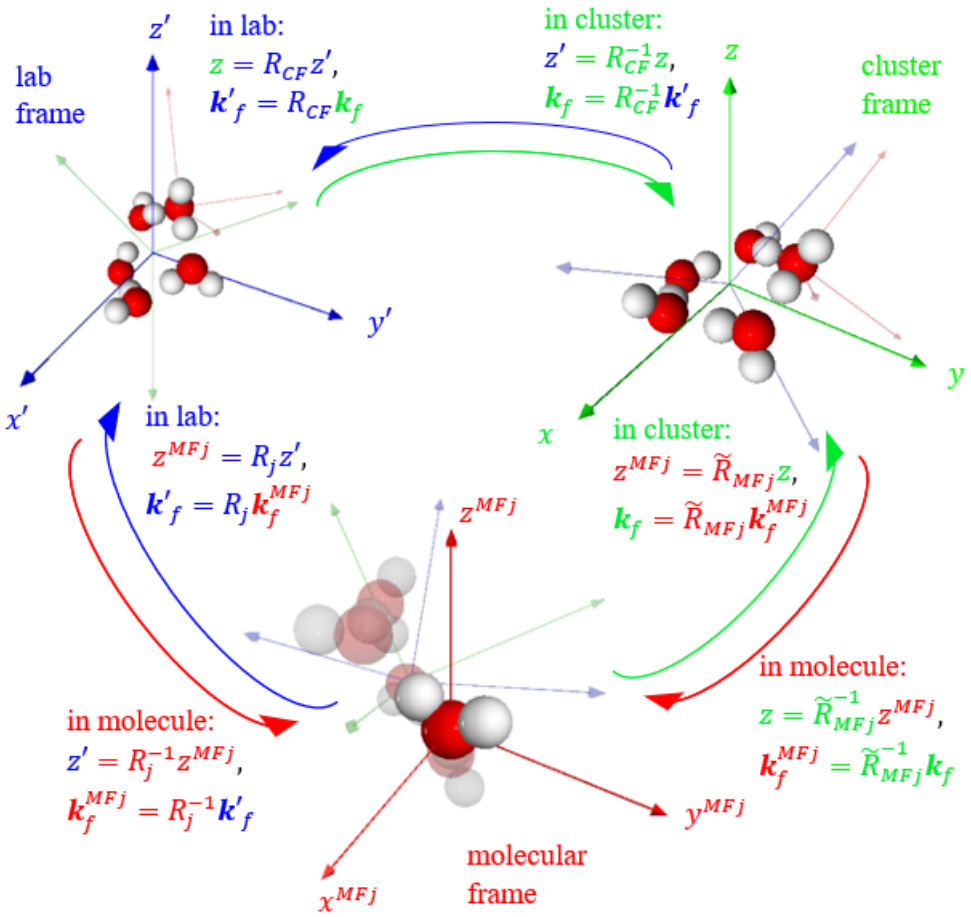

Figure 1.3: Illustration of the successive rotation $R_j = \tilde{R}_{MFj} R_{CF}$. The lab frame is blue, the cluster frame is green, the molecular frame is red. Basis vectors have the corresponding colors. The color of the signs of the photoelectron momentum vectors and of the equalities (=) matches the color of the frame in which they are defined. The Euler angles of R_{CF} are defined with respect to the lab frame and the angles of $\tilde{R}_{MFj}$ are defined with respect to the cluster frame. The text in the picture shows the formulae of the vector and axes transformations between each pair of the coordinate frames. The principle of the individual transformations (forward and inverse) is the same as in the case of rotations of a single molecule (see fig. 1.2).

before for one molecule, only here we need to deal with the extra phase factors and the composed rotation mentioned above. Expanding the modulus squared from eq. (1.89) and combining the exponentials gives:

$$\begin{aligned}
\left(\frac{\mathrm{d}\sigma}{\mathrm{d}\boldsymbol{k}'_f}\right)_{Av} &= 4\pi^2\alpha\omega\frac{1}{8\pi^2}\int \mathrm{d}R_{CF} \sum_{j=1}^{n}\sum_{j'=1}^{n} e^{\mathrm{i}(\boldsymbol{k}'_f\cdot\boldsymbol{\rho}'_j)} e^{-\mathrm{i}(\boldsymbol{k}'_f\cdot\boldsymbol{\rho}'_{j'})} \times \\
&\quad \times d'^{p}_{fi}(\boldsymbol{k}'_f, R_j)\left[d'^{p}_{fi}(\boldsymbol{k}'_f, R_{j'})\right]^* = \\
&= 4\pi^2\alpha\omega\frac{1}{8\pi^2}\int \mathrm{d}R_{CF} \sum_{j=1}^{n}\sum_{j'=1}^{n} e^{\mathrm{i}(\boldsymbol{k}'_f\cdot(\boldsymbol{\rho}'_j-\boldsymbol{\rho}'_{j'}))} \times \\
&\quad \times d'^{p}_{fi}(\boldsymbol{k}'_f, R_j)\left[d'^{p}_{fi}(\boldsymbol{k}'_f, R_{j'})\right]^* . \qquad (1.95)
\end{aligned}$$

The exponential factor can be expanded in spherical harmonics using the plane wave expansion (Cejnar [2013], p. 157, Varshalovich et al. [1988], p. 165):

$$e^{\mathrm{i}\boldsymbol{k}'_f\cdot\boldsymbol{\mathcal{R}}'_{jj'}} = 4\pi\sum_L\sum_{M=-L}^{L}\mathrm{i}^L j_L(k_f\mathcal{R}_{jj'})Y_{LM}(\boldsymbol{\mathcal{R}}'_{jj'})Y^*_{LM}(\boldsymbol{k}'_f), \tag{1.96}$$

where j_L is the L-th order spherical Bessel function, $\boldsymbol{\mathcal{R}}'_{jj'} = (\boldsymbol{\rho}'_j - \boldsymbol{\rho}'_{j'})$ is the difference between the position vectors of j-th and j'-th molecules and k and $\mathcal{R}'_{jj'}$ are their magnitudes. The lab frame vector $\boldsymbol{\mathcal{R}}'_{jj'}$ is related to the cluster-frame position vectors using the rotation R_{CF}:

$$\boldsymbol{\mathcal{R}}'_{jj'} = R_{CF}(\alpha_{CF},\beta_{CF},\gamma_{CF})\boldsymbol{\mathcal{R}}_{jj'} = R_{CF}(\alpha_{CF},\beta_{CF},\gamma_{CF})(\boldsymbol{\rho}_j - \boldsymbol{\rho}_{j'}). \tag{1.97}$$

In the next step we would like to expand the dipole matrix elements for each molecule in the cluster using the partial wave expansion (1.57) and couple the partial wave dipoles and spherical harmonics to perform the orientational averaging.

However, we must realize that the molecules in the cluster are not only rotated with respect to each other but also shifted (translated) with respect to the cluster center of mass. This introduces an additional complication in comparison to averaging for a single water molecule: to couple the spherical harmonics from mutually shifted molecular frames they all have to be expressed with respect to the same basis centered on the cluster center of mass. This can be achieved by translating the spherical harmonics from the molecular frame to the cluster frame (Varshalovich et al. [1988], p. 142):

$$\begin{aligned} Y_{lm}(\boldsymbol{r}_c) = Y_{lm}(\boldsymbol{r}+\boldsymbol{\rho}_j) = \sum_{l'=0}^{l}\left[\frac{4\pi(2l'+1)(2l-2l'+1)}{2l+1}\right]^{\frac{1}{2}} \\ \times\left(\frac{\rho_j}{r_c}\right)^l\left(\frac{r}{\rho_j}\right)^{l'}\sum_{m_1,m_2}C^{lm}_{l'm_1(l-l')m_2}Y_{l'm_1}(\boldsymbol{r})Y_{(l-l')m_2}(\boldsymbol{\rho}_j), \end{aligned} \tag{1.98}$$

where $\boldsymbol{r}_c$ denotes a position vector measured in the cluster frame and $\boldsymbol{r}$ a position vector in the molecular frame. However, as evident from these equations the translation depends on the radius r of the point $\boldsymbol{r}$ in the molecular frame. This means that to express the dipoles in the cluster frame we cannot use straightforwardly the dipoles generated in the spherical basis in the molecular frame since the radius r enters the integration over all space as implied by the definition of the partial wave dipole matrix element, see equation (1.44).

In order to perform the analytic averaging for the cluster we assume in the following that the partial wave dipole matrix elements have been generated in a solid spherical harmonic basis $S_{lm}(\boldsymbol{r})$ which is defined as (Helgaker et al. [2000], section 6.4.2):

$$S_{lm}(\boldsymbol{r}) = \sqrt{\frac{4\pi}{2l+1}}r^l Y_{lm}(\boldsymbol{r}). \tag{1.99}$$

When this basis is used the formula (1.98) takes the form:

$$S_{lm}(\boldsymbol{r}_c) = S_{lm}(\boldsymbol{r}+\boldsymbol{\rho}_j) = \sum_{l'=0}^{l}\sum_{m'=-l'}^{l'}\sum_{m''}A_{l'm'm''}(\boldsymbol{\rho}_j)S_{l',m'}(\boldsymbol{r})S_{l-l',m''}(\boldsymbol{\rho}_j), \tag{1.100}$$

where the coefficients $A_{l'm'm''}$ can be obtained from equation (1.98) after its multiplication by $\sqrt{\frac{4\pi}{2l+1}} r_c^l$. This translation formula has a trivial meaning: the solid harmonics are complex polynomials of order l (e.g. $S_{20}(\boldsymbol{r}) \sim 2z^2 - x^2 - y^2$) and their translation is therefore a linear combination of solid harmonics up to that order. Therefore the last formula can be employed to express the solid harmonics of the dipoles in the cluster frame, Δ^q_{lm}, using the solid harmonics of the dipoles from the molecular frame $d^{l_q q'}_{SH;l'm'}$:

$$\Delta^q_{lm} = \sum_{l'm'm''} \sum_{l_q=0}^{1} \sum_{q'q''} \left[A_{l'm'm''}(\boldsymbol{\rho}_j) S_{l-l',m''}(\boldsymbol{\rho}_j)\right]^* A_{l_q q' q''}(\boldsymbol{\rho}_j) S_{l-l_q,q''}(\boldsymbol{\rho}_j) d^{l_q q'}_{SH;l'm'}. \tag{1.101}$$

The translation can be neglected for the spherical harmonic of the photoelectron momentum $Y_{lm}(\boldsymbol{k}_f)$ which can be equivalently written in terms of a position of the electron on the detector: the detector is typically ≈ 1 m away from the interaction region while the displacement of a single molecule in the cluster is in the order of 10^{-10} m.

In the following we therefore assume that the molecular frame dipoles have been generated in the solid harmonic basis ($d^{l_q q'}_{SH;l'm'}$) and their angular parts have been translated into the cluster frame using equation (1.101). It is these dipoles Δ^q_{lm} which are used in the subsequent derivations.

The partial wave expansion of $\Delta'^p_{fi}(\boldsymbol{k}'_f, R_j)$ has exactly the form of equation (1.57). Using the formula (1.96) together with (1.57), we can rewrite the relation (1.95) as:

$$\begin{aligned}
\left(\frac{\mathrm{d}\sigma}{\mathrm{d}\boldsymbol{k}'_f}\right)_{Av} &= 4\pi^2 \alpha\omega \frac{1}{8\pi^2} \int \mathrm{d}R_{CF} \sum_{j=1}^{n} \sum_{j'=1}^{n} 4\pi \sum_{L,M} \mathrm{i}^L j_L(k_f \mathcal{R}_{jj'}) Y_{LM}(\boldsymbol{\mathcal{R}}'_{jj'}) \times \\
&\times Y^*_{LM}(\boldsymbol{k}'_f) \sum_{l,m} \sum_{\mu} Y_{l\mu}(\boldsymbol{k}'_f) D^l_{\mu,m}(R_j) \sum_q \left[D^1_{p,q}(R_j)\right]^* \Delta^q_{lm}(k_f) \times \\
&\times \sum_{l',m'} \sum_{\mu} Y^*_{l'\mu'}(\boldsymbol{k}'_f) \left[D^{l'}_{\mu',m'}(R_{j'})\right]^* \sum_{q'} D^1_{p,q'}(R_{j'}) \left[\Delta^{q'}_{l'm'}(k_f)\right]^*.
\end{aligned} \tag{1.102}$$

Now it is time to deal with the composed rotations R_j and $R_{j'}$. The same principle of basis transformation as described above for a rotational operator in the Cartesian basis by the equations (1.90)-(1.92) holds for any representation of the rotation operator. Therefore, the Wigner D-matrix of our composed rotation is (see Brink and Satchler [1968], Appendix V or Varshalovich et al. [1988], p. 33):

$$\begin{aligned}
\langle lm_1 | \tilde{R}_{MFj} R_{CF} | lm_2 \rangle &= D^l_{m_1,m_2}(\tilde{R}_{MFj} R_{CF}) = D^l_{m_1,m_2}(R_{CF} R_{MFj}) = \\
&= \sum_m D^l_{m_1,m}(R_{CF}) D^l_{m,m_2}(R_{MFj}).
\end{aligned} \tag{1.103}$$

Besides that we also need to express the spherical harmonics $Y_{LM}(\boldsymbol{\mathcal{R}}'_{jj'})$ depending on the direction of the vector $\boldsymbol{\mathcal{R}}'_{jj'} = \boldsymbol{\rho}'_j - \boldsymbol{\rho}'_{j'}$ using the vector $\boldsymbol{\mathcal{R}}_{jj'} = \boldsymbol{\rho}_j - \boldsymbol{\rho}_{j'}$ which does not depend on the rotation R_{CF}. In analogy with equations (1.48) and (1.50):

$$Y_{LM}(\boldsymbol{\mathcal{R}}'_{jj'}) = \sum_{M_Y} \left[D^L_{M,M_Y}(R_{CF})\right]^* Y_{LM_Y}(\boldsymbol{\mathcal{R}}_{jj'}). \tag{1.104}$$

Using the formula (1.103) and substituting the relation (1.104) into the expression (1.102) implies:

$$\left(\frac{\mathrm{d}\sigma}{\mathrm{d}\boldsymbol{k}'_f}\right)_{Av} = 4\pi^2\alpha\omega\frac{1}{8\pi^2}\int \mathrm{d}R_{CF}\sum_{j,j'}\sum_{L,M}\sum_{l,m}\sum_{l',m'}\sum_{\mu,\mu'}\sum_{q,q'} 4\pi \mathrm{i}^L j_L(k_f\mathcal{R}_{jj'})\times$$
$$\times Y^*_{LM}(\boldsymbol{k}'_f)Y_{l\mu}(\boldsymbol{k}'_f)Y^*_{l'\mu'}(\boldsymbol{k}'_f)\sum_{M_Y}\left[D^L_{M,M_Y}(R_{CF})\right]^* Y_{LM_Y}(\boldsymbol{\mathcal{R}}_{jj'})\times$$
$$\times\sum_{\mu_e} D^l_{\mu,\mu_e}(R_{CF})D^l_{\mu_e,m}(R_{MFj})\sum_{\mu_\gamma}\left[D^1_{p,\mu_\gamma}(R_{CF})\right]^*\left[D^1_{\mu_\gamma,q}(R_{MFj})\right]^*\times$$
$$\times\sum_{\mu'_e}\left[D^{l'}_{\mu',\mu'_e}(R_{CF})\right]^*\left[D^{l'}_{\mu'_e,m'}(R_{MFj'})\right]^*\sum_{\mu'_\gamma} D^1_{p,\mu'_\gamma}(R_{CF})D^1_{\mu'_\gamma,q'}(R_{MFj'})\times$$
$$\times\Delta^q_{lm}(k_f)\left[\Delta^{q'}_{l'm'}(k_f)\right]^*. \qquad (1.105)$$

Similarly as in case of one molecule, the expression (1.105) must be simplified before the orientational integral can be performed.

Again we will start by coupling the D-matrices depending on the orientation of the cluster R_{CF} of the photon and photoelectron angular momenta:

$$\left[D^1_{p,\mu_\gamma}(R_{CF})\right]^* D^1_{p,\mu'_\gamma}(R_{CF}) = (-1)^{p-\mu_\gamma}D^1_{-p,-\mu_\gamma}(R_{CF})D^1_{p,\mu'_\gamma}(R_{CF}) =$$
$$= (-1)^{p-\mu_\gamma}\sum_K(2K+1)\begin{pmatrix}1 & 1 & K\\ -p & p & M_K\end{pmatrix}\begin{pmatrix}1 & 1 & K\\ -\mu_\gamma & \mu'_\gamma & M'_K\end{pmatrix}\times$$
$$\times\left[D^K_{M_K,M'_K}(R_{CF})\right]^*, \qquad (1.106)$$

$$D^l_{\mu,\mu_e}(R_{CF})\left[D^{l'}_{\mu',\mu'_e}(R_{CF})\right]^* = (-1)^{\mu'-\mu'_e}D^l_{\mu,\mu_e}(R_{CF})D^{l'}_{-\mu',-\mu'_e}(R_{CF}) =$$
$$= (-1)^{\mu'-\mu'_e}\sum_\lambda(2\lambda+1)\begin{pmatrix}l & l' & \lambda\\ \mu & -\mu' & M_\lambda\end{pmatrix}\begin{pmatrix}l & l' & \lambda\\ \mu_e & -\mu'_e & M'_\lambda\end{pmatrix}\times$$
$$\times\left[D^\lambda_{M_\lambda,M'_\lambda}(R_{CF})\right]^*. \qquad (1.107)$$

Following these contractions we are left with only three D-matrices depending on R_{CF}. The integral $\int \mathrm{d}R_{CF}$ can be performed using the relation from Brink and Satchler [1968], Appendix V, for the angular integral over three Wigner D-matrices:

$$\int \mathrm{d}R_{CF}\left[D^L_{M,M_Y}(R_{CF})\right]^*\left[D^K_{M_K,M'_K}(R_{CF})\right]^*\left[D^\lambda_{M_\lambda,M'_\lambda}(R_{CF})\right]^* =$$
$$= \left[\int \mathrm{d}R_{CF}D^L_{M,M_Y}(R_{CF})D^K_{M_K,M'_K}(R_{CF})D^\lambda_{M_\lambda,M'_\lambda}(R_{CF})\right]^* =$$
$$= 8\pi^2\begin{pmatrix}L & K & \lambda\\ M & M_K & M_\lambda\end{pmatrix}\begin{pmatrix}L & K & \lambda\\ M_Y & M'_K & M'_\lambda\end{pmatrix}. \qquad (1.108)$$

And similarly as before, we must contract the spherical harmonics depending on the photoelectron momentum down to a single spherical harmonic. That can be done by contracting first $Y_{l\mu}(\boldsymbol{k}'_f)$ and $Y^*_{l'\mu'}(\boldsymbol{k}'_f)$, which is performed just the same way as before for one molecule (see eq. (1.67)):

$$Y_{l\mu}(\boldsymbol{k}'_f)Y^*_{l'\mu'}(\boldsymbol{k}'_f) = \sum_{L',M'}(-1)^{\mu'}\sqrt{\frac{(2l+1)(2l'+1)(2L'+1)}{4\pi}}\times$$
$$\times\begin{pmatrix}l & l' & L'\\ 0 & 0 & 0\end{pmatrix}\begin{pmatrix}l & l' & L'\\ \mu & -\mu' & M'\end{pmatrix}Y^*_{L'M'}(\boldsymbol{k}'_f), \qquad (1.109)$$

and then contracting this result with the remaining $Y^*_{LM}(\boldsymbol{k}'_f)$:

$$Y^*_{LM}(\boldsymbol{k}'_f)Y^*_{L'M'}(\boldsymbol{k}'_f) = \sum_{\Lambda,M_\Lambda}(-1)^{M+M'+M_\Lambda}\sqrt{\frac{(2L+1)(2L'+1)(2\Lambda+1)}{4\pi}}\times \\ \times\begin{pmatrix} L & L' & \Lambda \\ 0 & 0 & 0\end{pmatrix}\begin{pmatrix} L & L' & \Lambda \\ -M & -M' & -M_\Lambda\end{pmatrix}Y_{\Lambda M_\Lambda}(\boldsymbol{k}'_f). \quad (1.110)$$

Before substituting the results (1.106)-(1.110) into the relation (1.105) we can also get rid of some numerical factors. The factor 8π present in the result (1.108) is divided by the same number from the formula (1.105). The phase factor $(-1)^{\mu'}$ from (1.109) cancels with the same factor from (1.107). Finally, since M_Λ must satisfy the selection rule:

$$M_\Lambda = -M - M', \quad (1.111)$$

it is evident that the phase factor $(-1)^{M+M'+M_\Lambda}$ is always equal to 1. Realizing this and using the equations (1.106)-(1.110) gives:

$$\left(\frac{\mathrm{d}\sigma}{\mathrm{d}\boldsymbol{k}'_f}\right)_{Av} = 4\pi^2\alpha\omega\sum_{j,j'}\sum_{L,M}\sum_{l,m}\sum_{l',m'}\sum_{\mu,\mu'}\sum_{q,q'}\mathrm{i}^L j_L(k_f\mathcal{R}_{jj'})\sum_{M_Y}Y_{LM_Y}(\boldsymbol{\mathcal{R}}_{jj'})\times \\ \times\sum_{\mu_e,\mu'_e}\sum_{\mu_\gamma,\mu'_\gamma}D^l_{\mu_e,m}(R_{MFj})\left[D^1_{\mu_\gamma,\mu'_\gamma,q}(R_{MFj})\right]^*\left[D^{l'}_{\mu'_e,m'}(R_{MFj'})\right]^*D^1_{\mu'_\gamma,q'}(R_{MFj'})\times \\ \times\sum_{L',M'}\sum_{\Lambda,M_\Lambda}\sqrt{(2l+1)(2l'+1)(2L+1)(2\Lambda+1)}(2L'+1)(-1)^{p-\mu_\gamma+\mu'_e}\times \\ \times\sum_K\sum_\lambda(2K+1)(2\lambda+1)\begin{pmatrix} l & l' & L' \\ 0 & 0 & 0\end{pmatrix}\begin{pmatrix} l & l' & L' \\ \mu & -\mu' & M'\end{pmatrix}\begin{pmatrix} L & L' & \Lambda \\ 0 & 0 & 0\end{pmatrix}\times \\ \times\begin{pmatrix} L & L' & \Lambda \\ -M & -M' & -M_\Lambda\end{pmatrix}\begin{pmatrix} 1 & 1 & K \\ -p & p & M_K\end{pmatrix}\begin{pmatrix} 1 & 1 & K \\ -\mu_\gamma & \mu'_\gamma & M'_K\end{pmatrix}\begin{pmatrix} l & l' & \lambda \\ \mu & -\mu' & M_\lambda\end{pmatrix}\times \\ \times\begin{pmatrix} l & l' & \lambda \\ \mu_e & -\mu'_e & M'_\lambda\end{pmatrix}\begin{pmatrix} L & K & \lambda \\ M & M_K & M_\lambda\end{pmatrix}\begin{pmatrix} L & K & \lambda \\ M_Y & M'_K & M'_\lambda\end{pmatrix}Y_{\Lambda M_\Lambda}(\boldsymbol{k}'_f)\times \\ \times\Delta^q_{lm}(k_f)\left[\Delta^{q'}_{l'm'}(k_f)\right]^*. \quad (1.112)$$

Now one of the orthogonality relations between 3-j symbols (see Brink and Satchler [1968], Appendix I) can be used to get rid of two of the 3-j symbols from eq. (1.112):

$$\sum_{\mu,\mu'}(2L'+1)\begin{pmatrix} l & l' & L' \\ \mu & -\mu' & M'\end{pmatrix}\begin{pmatrix} l & l' & \lambda \\ \mu & -\mu' & M_\lambda\end{pmatrix} = \delta_{L'\lambda}\delta_{M'M_\lambda}. \quad (1.113)$$

The Kronecker deltas from this relation enable us to use the same orthogonality

relation between yet another pair of 3-j symbols:

$$\begin{aligned}
&\sum_{M,M'} (2K+1) \begin{pmatrix} L & K & \lambda \\ M & M_K & M_\lambda \end{pmatrix} \begin{pmatrix} L & L' & \Lambda \\ -M & -M' & -M_\Lambda \end{pmatrix} = \\
&= \sum_{M,M'} (2K+1) \begin{pmatrix} L & K & L' \\ M & M_K & M' \end{pmatrix} \begin{pmatrix} L & L' & \Lambda \\ -M & -M' & -M_\Lambda \end{pmatrix} = \\
&= \sum_{M,M'} (2K+1)(-1)^{L+L'+K} \begin{pmatrix} L & L' & K \\ M & M' & M_K \end{pmatrix} \begin{pmatrix} L & L' & \Lambda \\ -M & -M' & -M_\Lambda \end{pmatrix} = \\
&= \sum_{M,M'} (2K+1)(-1)^{2(L+L'+K)} \begin{pmatrix} L & L' & K \\ M & M' & M_K \end{pmatrix} \begin{pmatrix} L & L' & \Lambda \\ M & M' & M_\Lambda \end{pmatrix} = \\
&= \delta_{K\Lambda} \delta_{M_K M_\Lambda},
\end{aligned} \tag{1.114}$$

where we used the result (1.113) in the first step, the rule for swapping of the columns of a 3-j symbol (Brink and Satchler [1968], Appendix I) in the second step and the rule for changing the signs of the indices in the lower row of a 3-j symbol in the third step, which both give the same phase factor $(-1)^{L+L'+K}$, which therefore cancels out. And finally, the selection rules for 3-j symbols applied onto the first of the 3-j symbols from the relation (1.106) also imply:

$$\begin{aligned}
0 \leq K &\leq 2 \\
M_K &= -(p-p) = 0.
\end{aligned} \tag{1.115}$$

Combining the relations (1.113)-(1.115) together gives:

$$\begin{aligned}
\lambda &= L, \\
M_\lambda &= M', \\
0 \leq \Lambda &= K \leq 2, \\
M_\Lambda &= M_K = 0.
\end{aligned} \tag{1.116}$$

This leads to the coveted result:

$$Y_{\Lambda M_\Lambda}(\boldsymbol{k}'_f) = Y_{K M_K}(\boldsymbol{k}'_f) = Y_{K0}(\boldsymbol{k}'_f) = \sqrt{\frac{2K+1}{4\pi}} P_K(\cos\theta'), \tag{1.117}$$

where θ' is the angle measured from the lab-frame z' axis in agreement with the general formula (1.5).

Furthermore, the selection rules for the 3-j symbols can be used to determine two non-summation indices:

$$\begin{aligned}
M'_K &= \mu_\gamma - \mu'_\gamma, \\
M'_\lambda &= \mu'_e - \mu_e,
\end{aligned} \tag{1.118}$$

and also to get an important constraint on the M_Y summation index:

$$M_Y = -M'_K - M'_\lambda = -\mu_\gamma + \mu'_\gamma + \mu_e - \mu'_e. \tag{1.119}$$

This relation leaves only one nonzero term of the sum over M_Y and fixes this index. Therefore, the formula (1.112) can be finally rewritten in a needed simplified

form:

$$\left(\frac{\mathrm{d}\sigma}{\mathrm{d}\boldsymbol{k}'_f}\right)_{Av} = \frac{1}{4\pi}8\pi^{5/2}\alpha\omega\sum_K\sum_{j,j'}\sum_{L,L'}\sum_{l,m}\sum_{l',m'}\sum_{q,q'}\sum_{\mu_e,\mu'_e}\sum_{\mu_\gamma,\mu'_\gamma}\mathrm{i}^L j_L(k_f\mathcal{R}_{jj'})\times$$
$$\times Y_{LM_Y}(\boldsymbol{\mathcal{R}}_{jj'})D^l_{\mu_e,m}(R_{MFj})\left[D^1_{\mu_\gamma,q}(R_{MFj})\right]^*\left[D^{l'}_{\mu'_e,m'}(R_{MFj'})\right]^* D^1_{\mu'_\gamma,q'}(R_{MFj'})\times$$
$$\times\sqrt{(2l+1)(2l'+1)(2L+1)}(2L'+1)(2K+1)(-1)^{p-\mu_\gamma+\mu'_e}\times$$
$$\times\begin{pmatrix} l & l' & L' \\ 0 & 0 & 0\end{pmatrix}\begin{pmatrix} L & L' & K \\ 0 & 0 & 0\end{pmatrix}\begin{pmatrix} 1 & 1 & K \\ -p & p & 0\end{pmatrix}\begin{pmatrix} 1 & 1 & K \\ -\mu_\gamma & \mu'_\gamma & \mu_\gamma-\mu'_\gamma\end{pmatrix}\times$$
$$\times\begin{pmatrix} l & l' & L' \\ \mu_e & -\mu'_e & -\mu_e+\mu'_e\end{pmatrix}\begin{pmatrix} L & K & L' \\ M_Y & \mu_\gamma-\mu'_\gamma & -\mu_e+\mu'_e\end{pmatrix}P_K(\cos\theta')\times$$
$$\times\Delta^q_{lm}(k_f)\left[\Delta^{q'}_{l'm'}(k_f)\right]^*, \tag{1.120}$$

This is the expected result corresponding again to the general formula (1.5):

$$\left(\frac{\mathrm{d}\sigma}{\mathrm{d}\boldsymbol{k}'_f}\right)_{Av} = \frac{1}{4\pi}\sum_K A^c_K P_K(\cos\theta'), \tag{1.121}$$

where A^c_K, with the superscript c for cluster, embraces again all the other sums and the second constant factor. This yields the relations for the total cross section and the β parameters in the same form as in the equations (1.74)-1.76) before:

$$\sigma(E) = A^c_0, \tag{1.122}$$
$$\beta_1(E) = \frac{A^c_1}{A^c_0}, \tag{1.123}$$
$$\beta_2(E) = \frac{A^c_2}{A^c_0}. \tag{1.124}$$

Here, unlike for a single molecule which has two planes of symmetry, the β_1 parameter can potentially be nonzero in case of circularly polarized light (see Ritchie [1976]), because a molecular cluster as a whole in general can be a chiral object, depending on its exact geometric structure. Therefore, in principle, the derived relations could be used to calculate also β_1 as they include the case of circular polarization. However, the β_1 parameter is problematic since it is very sensitive to the effects that are neglected by the approximations within our IMM (see e.g. Powis [2000]). Thus any results for the β_1 parameter using the IMM would necessarily be very, even qualitatively inaccurate, which is why we focus only on the case of linearly polarized light.

1.3.3 Reality of the observables for a cluster

The photoelectron angular distribution is a real observable. However, the reality of the result (1.120) may not be clear at first sight and thus it deserves a detailed discussion.

Swapping of the indices jj' inverts the direction of the vector $\boldsymbol{\mathcal{R}}_{jj'}$ (see eq. (1.96)):

$$\boldsymbol{\mathcal{R}}_{j'j} = -\boldsymbol{\mathcal{R}}_{jj'}. \tag{1.125}$$

Because of the parity of the spherical harmonics (Varshalovich et al. [1988], p. 141):

$$Y_{LM_Y}(-\boldsymbol{\mathcal{R}}_{jj'}) = (-1)^L Y_{LM_Y}(\boldsymbol{\mathcal{R}}_{jj'}), \tag{1.126}$$

the relation (1.125) implies that swapping of the j-th and j'-th molecule in the summations over jj' gives an additional phase factor $(-1)^L$ changing the factor i^L to $(-i)^L$. The D-matrices belonging to the j-th and j'-th molecule also switch, which exchanges the primed and unprimed μ-indices. Therefore, the equation (1.119) ensures that swapping of the molecules also changes the sign of the index M_Y. This together with the phase factor $(-1)^{-\mu_\gamma+\mu'_e}$ and the relation for complex conjugation of the spherical harmonics (Varshalovich et al. [1988], p. 140) implies:

$$\begin{aligned}(-1)^{-\mu_\gamma+\mu'_e} Y_{L-M_Y}(\boldsymbol{\mathcal{R}}_{jj'}) &= (-1)^{-\mu_\gamma+\mu'_e-M_Y} Y^*_{LM_Y}(\boldsymbol{\mathcal{R}}_{jj'}) = \\ &= (-1)^{-\mu'_\gamma+\mu_e} Y^*_{LM_Y}(\boldsymbol{\mathcal{R}}_{jj'}).\end{aligned} \tag{1.127}$$

This means that swapping of the j-th and j'-th molecules is equivalent to complex conjugation of the terms non-diagonal in jj' indices, leaving only summations of the type $z + z^* = 2Re(z)$.

The diagonal terms of the summation over molecules are also real. For $j = j'$ we have $\boldsymbol{\mathcal{R}}_{jj'} = \boldsymbol{\mathcal{R}}_{jj} = \vec{0}$, implying:

$$\mathrm{i}^L j_L(k_f \mathcal{R}_{jj'}) Y_{LM_Y}(\boldsymbol{\mathcal{R}}_{jj'})\Big|_{j=j'} = \frac{1}{\sqrt{4\pi}}, \tag{1.128}$$

because asymptotically (Cejnar [2013], p. 170):

$$j_L(0) = \begin{cases} 1, & L = 0, \\ 0, & L > 0. \end{cases} \tag{1.129}$$

Therefore $L = 0$ and thus

$$Y_{LM_Y} = Y_{00} = \frac{1}{\sqrt{4\pi}}, \tag{1.130}$$

with $\mathrm{i}^L = \mathrm{i}^0 = 1$. This factor is real and the summation of the products of the four Wigner D-matrix elements reduces itself to the sum of numbers in the form of $z + z^* = 2Re(z)$ or $zz^* = |z|^2$ in case of $j = j'$.

This shows that the final result (1.120) is a real observable as it should.

1.3.4 Reduction of the result for a cluster to the case of a single molecule

Here we show that the result (1.120) is a generalisation of eq. (1.72) for a single molecule. For $n = 1$, only the diagonal term with $j = j' = 1$ contributes. In that case:

$$L = 0 \Rightarrow M_Y = 0 \tag{1.131}$$

and the factor including the spherical Bessel function and a spherical harmonic from the plane wave expansion (1.96) is reduced to $1/\sqrt{4\pi}$ (see eq. (1.129)-(1.130)).

To deal with the D-matrices depending on R_{MFj}, we could couple them using the same relations as (1.61)-(1.62) or (1.106)-(1.107). However, a much easier approach is to identify the cluster frame with the molecular frame, which surely can be done since there is only one molecule. This reduces the dipoles Δ^q_{lm} from eq. (1.101) back to d^q_{lm} and all the Wigner matrices $D(R_{MFj})$ to identity matrices (Kronecker deltas), which implies:

$$\begin{aligned} \mu_e &= m, \\ \mu'_e &= m', \\ \mu_\gamma &= q, \\ \mu'_\gamma &= q'. \end{aligned} \tag{1.132}$$

These constraints remove the summations over $\mu_e, \mu'_e, \mu_\gamma$ and μ'_γ and together with the equations (1.131) and (1.119) they also imply:

$$0 = M_Y = -q + q' + m - m' \Longrightarrow m - m' = q - q'. \tag{1.133}$$

Therefore the result for the photoelectron angular distribution is reduced to:

$$\begin{aligned} &\left(\frac{\mathrm{d}\sigma}{\mathrm{d}\boldsymbol{k}'_f}\right)_{Av}\Bigg|_{n=1} = \frac{1}{4\pi} 4\pi^2 \alpha\omega \sum_K \sum_{L'} \sum_{l,m} \sum_{l',m'} \sum_{q,q'} (2L'+1)(2K+1) \times \\ &\times \sqrt{(2l+1)(2l'+1)} (-1)^{p-q+m'} \begin{pmatrix} l & l' & L' \\ 0 & 0 & 0 \end{pmatrix} \begin{pmatrix} 0 & L' & K \\ 0 & 0 & 0 \end{pmatrix} \begin{pmatrix} 1 & 1 & K \\ -p & p & 0 \end{pmatrix} \times \\ &\times \begin{pmatrix} 1 & 1 & K \\ -q & q' & m-m' \end{pmatrix} \begin{pmatrix} l & l' & L' \\ m & -m' & -m+m' \end{pmatrix} \begin{pmatrix} 0 & K & L' \\ 0 & m-m' & -m+m' \end{pmatrix} \times \\ &\times P_K(\cos\theta') d^q_{lm}(k_f) \left[d^{q'}_{l'm'}(k_f) \right]^*, \end{aligned} \tag{1.134}$$

The selection rules for the second and the last Wigner 3-j symbol imply that:

$$L' = K. \tag{1.135}$$

However, the forms of the 3-j symbols containing zero angular momentum are explicitly known (Brink and Satchler [1968], Appendix I):

$$\begin{pmatrix} A & B & 0 \\ a & b & 0 \end{pmatrix} = (-1)^{A-a} \delta_{AB} \delta_{a-b} \frac{1}{\sqrt{2A+1}}. \tag{1.136}$$

With this relation and with the rules for swapping of the columns of the 3-j symbols (Brink and Satchler [1968], Appendix I), the two 3-j symbols can be explicitly rewritten as:

$$\begin{pmatrix} 0 & L' & K \\ 0 & 0 & 0 \end{pmatrix} = \begin{pmatrix} L' & K & 0 \\ 0 & 0 & 0 \end{pmatrix} = (-1)^{L'} \delta_{L'K} \delta_{00} \frac{1}{\sqrt{2L'+1}}, \tag{1.137}$$

$$\begin{aligned} &\begin{pmatrix} 0 & K & L' \\ 0 & m-m' & -m+m' \end{pmatrix} = \begin{pmatrix} K & L' & 0 \\ m-m' & -m+m' & 0 \end{pmatrix} = \\ &= (-1)^{K-m+m'} \delta_{KL'} \frac{1}{\sqrt{2K+1}}, \end{aligned} \tag{1.138}$$

where in the last step we used $\delta_{(m-m')-(-m+m')} = 1$. Put together these relations yield:

$$\begin{pmatrix} 0 & L' & K \\ 0 & 0 & 0 \end{pmatrix} \begin{pmatrix} 0 & K & L' \\ 0 & m-m' & -m+m' \end{pmatrix} = (-1)^{m'-m} \frac{1}{2K+1}, \tag{1.139}$$

where we used $(-1)^{L'+K} = (-1)^{2K} = 1$. Hence, the final result in case of $n = 1$ is:

$$\begin{aligned} &\left(\frac{\mathrm{d}\sigma}{\mathrm{d}\boldsymbol{k}'_f}\right)_{Av}\Bigg|_{n=1} = \frac{1}{4\pi} 4\pi^2 \alpha\omega \sum_K \sum_{l,m} \sum_{l',m'} \sum_{q,q'} (2K+1) \times \\ &\times \sqrt{(2l+1)(2l'+1)} (-1)^{p-q-m} \begin{pmatrix} l & l' & K \\ 0 & 0 & 0 \end{pmatrix} \begin{pmatrix} 1 & 1 & K \\ -p & p & 0 \end{pmatrix} \times \\ &\times \begin{pmatrix} 1 & 1 & K \\ -q & q' & m-m' \end{pmatrix} \begin{pmatrix} l & l' & K \\ m & -m' & m'-m \end{pmatrix} \times \\ &\times P_K(\cos\theta') d^q_{lm}(k_f) \left[d^{q'}_{l'm'}(k_f)\right]^* . \end{aligned} \tag{1.140}$$

And since the equation (1.133) implies:

$$(-1)^{p-q-m} = (-1)^{p+q-m} = (-1)^{p+q'-m'}, \tag{1.141}$$

it is evident, that the result (1.140) is equivalent (1.72).

2. Results and discussion

In this chapter the results of calculations using the theoretical model developed above are presented. Since the β_1 parameter is very sensitive to the effects neglected by our IMM (Powis [2000]), we focused on the case of the ionization by linearly polarized light in which β_1 is equal to zero (Ritchie [1976]), as mentioned at the end of Subsection 1.3.2. Results for a single H_2O molecule, obtained using the analytic relations (1.72), (1.74) and (1.76), are verified using the numerical results and reference data which were provided by my supervisor Dr. Zdeněk Mašín. The results for small $(H_2O)_n$ clusters are presented after that and the dependence of the results on cluster geometries is studied. First of all, the input data and the numerical method used for the orientational averaging are described.

2.1 Structure of the input partial wave dipole elements

The input data containing the partial wave dipole moments for a single H_2O molecule were supplied by my supervisor, who obtained them from the code UKRmol+ (Mašín et al. [2020]). The provided partial wave dipoles were generated for the angular momenta l in the range $0 \leq l \leq 6$ and for 700 photon energies evenly spaced in the range from 13.403 eV to 82.403 eV, where the lower value corresponds to the ionization potential of the $1b_1$ orbital, i.e. the minimal energy needed to release the electron. In this subsection we will briefly summarize the different forms of the dipoles output by this code.

The UKRmol+ code uses the basis of real spherical harmonics, see Blanco et al. [1997], for both the photoelectron momentum and the photon polarization and produces the dipoles in the KET form for the photoelectron wave function:

$$\mathbf{d}_{fi}(\boldsymbol{k}_f)^{KET} = \langle \Psi_i | \hat{\mathbf{d}} | \Psi^{(-)}_{f,\boldsymbol{k}_f} \rangle, \tag{2.1}$$

$$\hat{\mathbf{d}} = (\hat{d}_x, \hat{d}_y, \hat{d}_z). \tag{2.2}$$

Consequently, these dipole matrix elements are expanded into partial wave dipoles using the real spherical harmonics X_{lm}:

$$\mathbf{d}_{fi}(\boldsymbol{k}_f)^{KET} = \langle \Psi_i | \hat{\mathbf{d}} | \Psi^{(-)}_{f,\boldsymbol{k}_f} \rangle = \sum_{l,m} \mathrm{i}^l e^{-\mathrm{i}\sigma_l} X_{lm}(\boldsymbol{k}_f) \mathbf{d}^{COMPAK}_{lm} = \tag{2.3}$$

$$= \sum_{l,m} X_{lm}(\boldsymbol{k}_f) \mathbf{d}^{DIPOLE-TOOLS}_{lm}, \tag{2.4}$$

where $\mathbf{d}^{COMPAK}_{lm}$ are the partial wave dipole matrix elements returned by the code `COMPAK` and $\mathbf{d}^{DIPOLE-TOOLS}_{lm}$ are partial wave dipoles returned by the code `DIPOLE_TOOLS`, where both of these codes are subprograms of the code UKRmol+. The elements $\mathbf{d}^{DIPOLE-TOOLS}_{lm}$ absorb the phase factors from the partial wave expansion:

$$\mathbf{d}^{DIPOLE-TOOLS}_{lm} = \mathrm{i}^l e^{-\mathrm{i}\sigma_l} \mathbf{d}^{COMPAK}_{lm}, \tag{2.5}$$

in agreement with the convention introduced in Chapter 1, eq. (1.57).

The molecular coordinate frame, in which the UKRmol+ calculations were performed, is depicted in figure 2.1. The z-axis is aligned with the C_2 axis of symmetry of the water molecule and the yz plane of symmetry σ_{yz} contains both hydrogen atoms. The same form of the molecular frame is used in all illustrations of the coordinate frames throughout the entire thesis.

The lab-frame photoionization amplitude can be written as:

$$\begin{aligned} a_{fi}^{\boldsymbol{\xi}'}(\boldsymbol{k}'_f) &= \boldsymbol{\xi}'\cdot \mathbf{d}'_{fi}(\boldsymbol{k}'_f, R)^{KET} = \boldsymbol{\xi}\cdot \mathbf{d}_{fi}(\boldsymbol{k}_f)^{KET} = & (2.6)\\ &= (R^{-1}\boldsymbol{\xi}')\cdot \mathbf{d}_{fi}(R^{-1}\boldsymbol{k}'_f)^{KET} = & (2.7)\\ &= \sum_{l,m} X_{lm}(R^{-1}\boldsymbol{k}'_f)\left[\mathbf{d}_{lm}^{DIPOLE-TOOLS}\cdot (R^{-1}\boldsymbol{\xi}')\right], & (2.8) \end{aligned}$$

which allows to express the lab-frame dipole using the quantities generated by the UKRmol+ code. These forms can be used to perform the numerical calculation as described in the following subsection. However, the analytic results derived in Chapter 1 use the BRA form of the dipole matrix elements and the basis of complex spherical harmonics. Therefore, to ensure consistency with the analytic results, the dipoles output by the `DIPOLE_TOOLS` code must be transformed into their BRA forms and into the basis of complex spherical harmonics for both the photoelectron momentum and the photon polarization. This is performed using the relation:

$$d_{l\mu}^{q} = \sum_{m'}\sum_{q'} (C^{1}_{q,q'})^{-1}\left[(C^{l}_{\mu,m'})^{-1}\right]^{*}\left[d_{lm'}^{q',DIPOLE-TOOLS}\right]^{*}, \qquad (2.9)$$

where $C^{l}_{\mu,m'}$ are elements of the unitary transformation matrix $\mathbf{C}^{l}$ which are given explicitly in the paper by Blanco et al. [1997]. These transformed partial wave

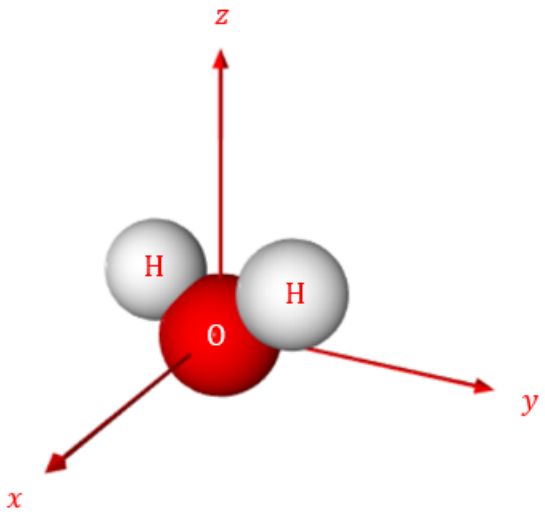

Figure 2.1: The molecular frame chosen for the construction of the dipole matrix elements (cf. the orbital $1b_1$ depicted in figure 2). The oxygen atom is red, the hydrogen atoms are white. The origin is identified with the center of mass of the molecule and all the atoms lie in the yz plane. The same geometry of the molecular frame was used in all the previous figures illustrating the rotations and will be used in all the following figures depicting the cluster geometry.

dipole matrix elements $d^q_{l\mu}(k_f)$ are those entering the equation (1.57), hence these are used to perform the analytic calculations for a single molecule.

For clusters the main results were generated using the numerical averaging procedure. The analytic calculation requires dipoles generated in the basis of solid harmonics for reasons explained in the Subsection 1.3.2. However, the UKRmol+ code that we use to generate the partial wave dipoles is not able to work in the basis of solid harmonics. Therefore we could not produce consistent results for clusters using analytic averaging in this work.

2.2 Description of the numerical calculation

To perform the orientional averaging for a single molecule numerically, we use the relation (1.24) together with the equations (2.6)–(2.8):

$$\left(\frac{\mathrm{d}\sigma}{\mathrm{d}\boldsymbol{k}'_f}\right)_{Av} = 4\pi^2\alpha\omega\frac{1}{8\pi^2}\int \mathrm{d}R \left|\boldsymbol{\xi}'\mathbf{d}'_{fi}(\boldsymbol{k}'_f,R)^{KET}\right|^2 = \tag{2.10}$$

$$= \frac{\alpha\omega}{2}\int \mathrm{d}R \left|(R^{-1}\boldsymbol{\xi}')\cdot\mathbf{d}_{fi}(R^{-1}\boldsymbol{k}'_f)^{KET}\right|^2 = \tag{2.11}$$

$$= \frac{\alpha\omega}{2}\int \mathrm{d}R \left|\sum_{l,m} X_{l,m}(R^{-1}\boldsymbol{k}'_f)\left[\mathbf{d}^{DIPOLE-TOOLS}_{lm}\cdot(R^{-1}\boldsymbol{\xi}')\right]\right|^2, \tag{2.12}$$

where α from equations (2.10)–(2.12) is the fine structure constant not to be confused with the Euler angle α bellow. The symbol $\int \mathrm{d}R$ stands for the integral over all orientations of the molecule:

$$\int \mathrm{d}R = \int_0^{2\pi}\mathrm{d}\alpha\int_0^{\pi}\sin(\beta)\mathrm{d}\beta\int_0^{2\pi}\mathrm{d}\gamma. \tag{2.13}$$

For molecular clusters, the numerical calculation is performed identically, only the integrand is the square of the coherent superposition of dipoles resulting from the independent molecule model (see eq. (1.88)) and the averaging over all orientations R_{CF} of the cluster frame:

$$\left(\frac{\mathrm{d}\sigma}{\mathrm{d}\boldsymbol{k}'_f}\right)_{Av} = \frac{\alpha\omega}{2}\int \mathrm{d}R_{CF}\times$$

$$\times\left|\sum_{l,m}\sum_{j=1}^{n} e^{\mathrm{i}[(R^{-1}_{CF}\boldsymbol{k}'_f)\cdot\boldsymbol{\rho}_j]}X_{l,m}(R_j^{-1}\boldsymbol{k}'_f)\left[\mathbf{d}^{DIPOLE-TOOLS}_{lm}\cdot(R_j^{-1}\boldsymbol{\xi}')\right]\right|^2. \tag{2.14}$$

Note that the dipole for each molecule is evaluated using an independent partial wave expansion in the molecular frame of each molecule in the basis of real spherical harmonics depending on the direction of the photoelectron momentum $\boldsymbol{k}_f^{MFj} = R_j^{-1}\boldsymbol{k}'_f$. Therefore, the translation of the molecular frames does not cause a problem in the numerical calculation.

The 3D integral above can be written as a sequence of two integrations, a 1D integral over α and a 2D integral over β and γ:

$$\left(\frac{\mathrm{d}\sigma}{\mathrm{d}\boldsymbol{k}'_f}\right)_{Av} = \frac{\alpha\omega}{2}\int \mathrm{d}R_{CF} f(\alpha,\beta,\gamma) = \int_0^{2\pi}\mathrm{d}\alpha g(\alpha), \tag{2.15}$$

$$g(\alpha) = \int_0^{\pi}\sin(\beta)\mathrm{d}\beta\int_0^{2\pi}\mathrm{d}\gamma f(\alpha,\beta,\gamma), \tag{2.16}$$

where the integrand $f(\alpha, \beta, \gamma)$ is

$$f(\alpha, \beta, \gamma) = \left| \sum_{l,m} \sum_{j=1}^{n} e^{\mathrm{i}[(R_{CF}^{-1}\boldsymbol{k}'_f)\cdot\boldsymbol{\rho}_j]} X_{l,m}(R_j^{-1}\boldsymbol{k}'_f) \left[\mathbf{d}_{lm}^{DIPOLE-TOOLS} \cdot (R_j^{-1}\boldsymbol{\xi}')\right] \right|^2. \tag{2.17}$$

Our initial attempt was to use fixed-order 1D and 2D quadratures to perform the 3D integral. The outer 1D integral over α can be approximated straightforwardly by a Gauss-Legendre quadrature:

$$\left(\frac{\mathrm{d}\sigma}{\mathrm{d}\boldsymbol{k}'_f}\right)_{Av} = \int_0^{2\pi} \mathrm{d}\alpha g(\alpha) \approx \sum_{j=1}^{N} w_j g(\alpha_j), \tag{2.18}$$

where N is the order of the Gauss-Legendre rule and w_j are the corresponding quadrature weights for the interval $[0; 2\pi]$. The integral (2.16) has the form of an integral over sphere which can be approximated by the Lebedev quadrature (see Lebedev [1976]) which is a generalization of the Gauss-Legendre quadrature rule to sphere:

$$g(\alpha) = \int_0^{\pi} \sin(\beta)\mathrm{d}\beta \int_0^{2\pi} \mathrm{d}\gamma f(\alpha, \beta, \gamma) \approx \frac{1}{4\pi} \sum_{i=1}^{N_L} w_i^L f(\alpha, \beta_i, \gamma_i), \tag{2.19}$$

where N_L is the order of the Lebedev rule, w_i^L are the quadrature weights and (β_i, γ_i) are the quadrature points. A Lebedev rule of order N_L is constructed to integrate exactly a spherical harmonic of angular momentum N_L.

However, using the fixed-point quadrature rules has proved impractical: the integrand $f(\alpha, \beta, \gamma)$ has sharp spikes which are difficult to integrate over with a fixed-point Lebedev rule. Therefore we abandoned this approach and replaced the fixed-point 1D and 2D quadratures with their adaptive versions based on Gauss-Legendre quadrature rules using a FORTRAN code developed by my supervisor. These codes require on input the parameters for the required relative precisions ϵ_α and $\epsilon_{\beta,\gamma}$ of the 1D and 2D integrals respectively. Since we're computing an observable (cross-section) a very high relative precision of the result is not needed. Therefore, it was sufficient to use $\epsilon_\alpha = 10^{-3}$ and $\epsilon_{\beta,\gamma} = 10^{-4}$. The numerical quadrature has to be performed for each choice of the lab-frame polarization $\boldsymbol{\xi}'$ and the lab-frame electron momentum $\boldsymbol{k}'_f$. We have chosen the lab-frame polarization to point along the z'-axis while the directions of the lab-frame electron momenta were taken from a Lebedev quadrature of order 4. Using this procedure we explicitly generated, for each chosen photon energy, the photoelectron angular distribution $(\frac{\mathrm{d}\sigma}{\mathrm{d}\boldsymbol{k}'_f})_{Av}$ on a grid of lab-frame photoelectron directions.

The general form of the photoelectron angular distribution is given by the equation (1.5) and since we focus only on the case of ionization by the linearly polarized light when the parameter β_1 is equal to 0, the formula is reduced to:

$$\left(\frac{\mathrm{d}\sigma}{\mathrm{d}\boldsymbol{k}'_f}\right)_{Av} = \frac{\sigma(E)}{4\pi} \left(1 + \beta_2(E) P_2(\cos\theta')\right). \tag{2.20}$$

If the differential cross section $(\frac{\mathrm{d}\sigma}{\mathrm{d}\boldsymbol{k}'_f})_{Av}$ is integrated over all directions of the $\boldsymbol{k}'_f$ vector in the lab, i.e. over the full solid angle in the lab frame, the result is:

$$\int \mathrm{d}\Omega_{\boldsymbol{k}'_f} \left(\frac{\mathrm{d}\sigma}{\mathrm{d}\boldsymbol{k}'_f}\right)_{Av} = \frac{\sigma(E)}{4\pi}. \tag{2.21}$$

Doing the same but with the integrand multiplied by the second order Legendre polynomial $P_2(\cos(\theta'))$, where θ' is the angle measured from the lab-frame z' axis (see Section 1.2.4), we get:

$$\int \mathrm{d}\Omega_{\boldsymbol{k}'_f} \left(\frac{\mathrm{d}\sigma}{\mathrm{d}\boldsymbol{k}'_f}\right)_{Av} P_2(\cos(\theta')) = \frac{\beta_2(E)\sigma(E)}{4\pi}. \tag{2.22}$$

These integrals can be calculated exactly using the fixed-order Lebedev quadrature. Comparing the equations (2.21) and (2.22), it is clear that the β_2 parameter can be calculated as:

$$\beta_2(E) = \frac{\int \mathrm{d}\Omega_{\boldsymbol{k}'_f} (\frac{\mathrm{d}\sigma}{\mathrm{d}\boldsymbol{k}'_f})_{Av} P_2(\cos(\theta'))}{\int \mathrm{d}\Omega_{\boldsymbol{k}'_f} (\frac{\mathrm{d}\sigma}{\mathrm{d}\boldsymbol{k}'_f})_{Av}} = \frac{\frac{1}{4\pi}\sum_i w_i^L (\frac{\mathrm{d}\sigma}{\mathrm{d}\boldsymbol{k}'_i})_{Av} P_2(\cos\theta'_i)}{\frac{1}{4\pi}\sum_j w_j^L (\frac{\mathrm{d}\sigma}{\mathrm{d}\boldsymbol{k}'_j})_{Av}}. \tag{2.23}$$

The numerical calculations were used to verify the results obtained analytically using the relation (1.72) for a single molecule and to obtain the main results for small water clusters.

2.3 Results for a single water molecule

The cross sections $\sigma(E)$ and beta-parameters $\beta_2(E)$ for a single molecule were calculated for photon energies in range from the ionization potential 13.403 eV to 82.403 eV. The analytic results were calculated for all 700 energies using my own code written in Python 2.7. The numerical calculation using the adaptive quadratures was performed by the code written by my supervisor in FORTRAN 90 but only for 70 energies (every 10th from those 700) in order to speed up the calculation. This code was based on my original Python implementation of the numerical averaging which used the fixed-order 1D and 2D quadratures.

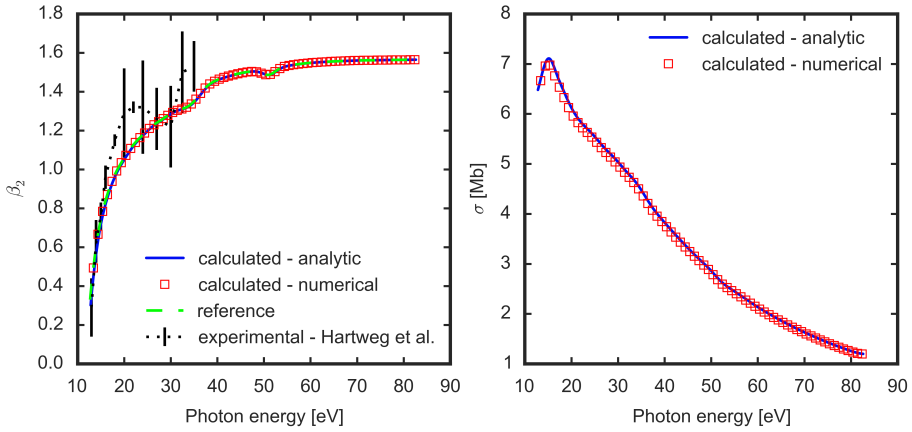

Figure 2.2: Results for a single H_2O molecule. The β_2 parameters are in the left panel, the cross sections σ are in the right panel. For the asymmetry parameter β_2 both analytic and numerical results are compared with the reference values calculated by the code UKRmol+ and experimental results from Hartweg et al. [2017].

First we calculated $\sigma(E)$ and $\beta_2(E)$ using all the angular momenta $0 \leq l \leq 6$ for which we had the dipole moments. Both the numerical and the analytic results of this calculation are shown in figure 2.2. The results calculated analytically

using the relations (1.72) and (1.74), (1.76) are compared with the numerical results calculated by the equations (2.21) and (2.23). The β_2 parameters, which are in the left panel of figure 2.2, are also compared with the experimental results from the Supporting Information for Hartweg et al. [2017] and with the reference values obtained by the code UKRmol+ in order to test the precision of our calculations. All our calculated results are in agreement with each other and with the experimental results from Hartweg et al. [2017] within the error bars of the experiment or close to them in the low energy range bellow 20 eV. This confirms that the relations (1.72)-(1.76) derived by us are correct. The reason for larger experimental values around 20-25 eV and 35 eV are the autoionizing resonances (Friedrich [2006], section 3.3.2) which are effectively removed from the dipoles from the code UKRmol+ by a smoothing procedure, see Mašín et al. [2020].

We also tested the convergence of the analytic expression (1.72) with the angular momentum l. These results are shown in figure 2.3. It is clear that both σ and β_2 are well converged already for $l_{max} = 3$. The reason for this is that the chosen molecular orbital $1b_1$, see fig. 2, is very similar to the atomic p orbital ($l = 1$) which, due to the dipole selection rules implied by the equations (1.44)-(1.45), can be ionized either to an s orbital ($l = 0$) or to a d orbital ($l = 2$). The clear dominance of the $l = 2$ contribution is in agreement with the general Fano propensity rule which states that the transitions $l \to l+1$ are much stronger than $l \to l-1$, see Fano [1985]. The contributions of the higher angular momenta l are corrections caused by the presence of the hydrogen atoms in the H_2O molecule. This suggests that the results for clusters will also converge for around $l = 3$, however this must be tested as well.

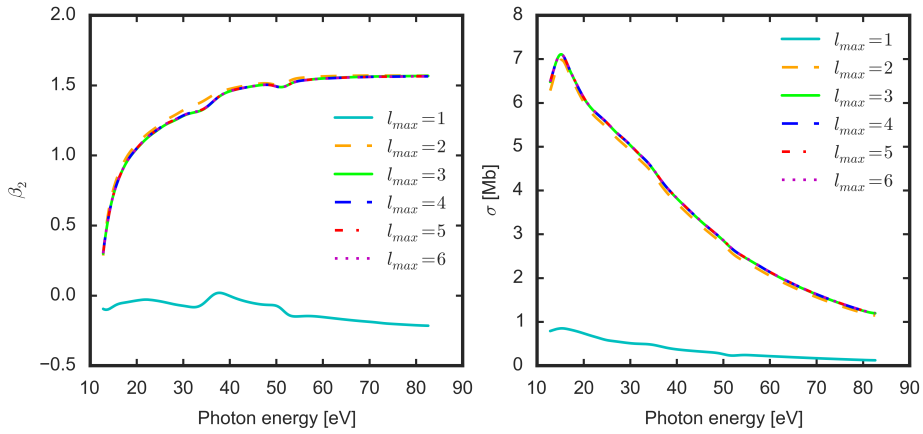

Figure 2.3: Results of the test of convergence of the analytic calculation with l for a single H_2O molecule.

2.4 Results for small water clusters

In this section we present the results calculated using the IMM for a few of the geometric structures of the small water clusters taken from the database of Rakshit et al. [2019b]. The results were calculated numerically using the equations (2.14)-(2.23). The IMM depends on several parameters: on the positions of the molecules in the cluster and on their orientation. In this section we explore

the dependence on these parameters and on the convergence of the partial wave expansion for the dipoles.

2.4.1 Geometries of the water clusters

The files from Rakshit et al. [2019b] contain the Cartesian coordinates of each atom of the cluster. From that, we calculate the position of the cluster center of mass and then translate the origin into that point. This creates the cluster frame. The individual molecular frames are then calculated similarly with their origins identified with the centers of mass of the corresponding molecules (the vectors $\boldsymbol{\rho}_j$). The Euler angles of the molecular frame axes in the cluster frame are then found using a procedure described bellow, using the $z-y-z$ convention of the successive rotations of the molecular frame from the cluster frame by the Euler angles as described in the Subsection 1.2.3 or in Varshalovich et al. [1988], section 1.4.1. An example of the cluster geometry is depicted in figure 2.4.

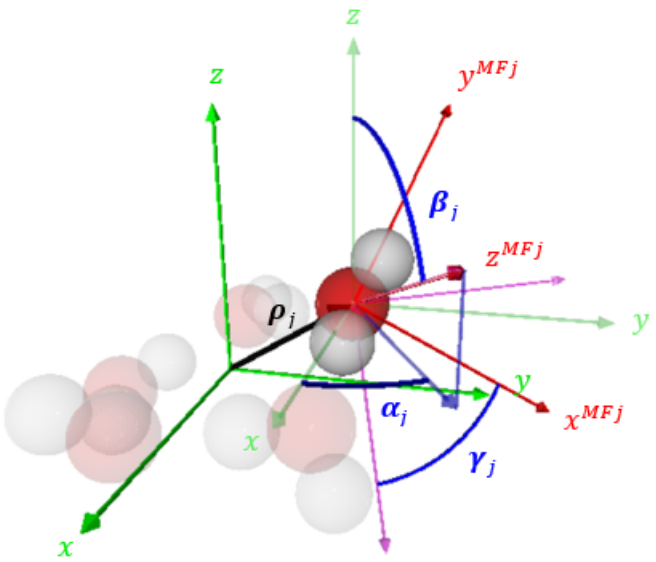

Figure 2.4: Illustration of the geometry of $(H_2O)_5$ cluster. The cluster frame is green, the molecular frame is red. The position vector of the molecule in the cluster frame $\boldsymbol{\rho_j}$ is black. The Euler angles of the molecule with respect to the cluster frame are blue.

The angles $\alpha_{MFj}, \beta_{MFj}$ are calculated directly as the spherical coordinates of the z^{MFj} axis in the cluster frame:

$$\beta_{MFj} = \arccos\left((z^{MFj})_z\right), \tag{2.24}$$

$$\alpha_{MFj} = \arctan\left(\frac{(z^{MFj})_y}{(z^{MFj})_x}\right), \tag{2.25}$$

where both equations are written in the cluster frame and $(z^{MFj})_x$, $(z^{MFj})_y$, $(z^{MFj})_z$ are the components of the molecular frame $\boldsymbol{z}^{MFj} = R_{MFj}\boldsymbol{z}$ basis vector in the cluster frame basis. This basis vector is obtained simply as the sum of the position vectors of the hydrogen atoms in the cluster frame shifted into the center of mass of the j-th molecule (cf. figures 2.1 and 2.4). Then the matrix

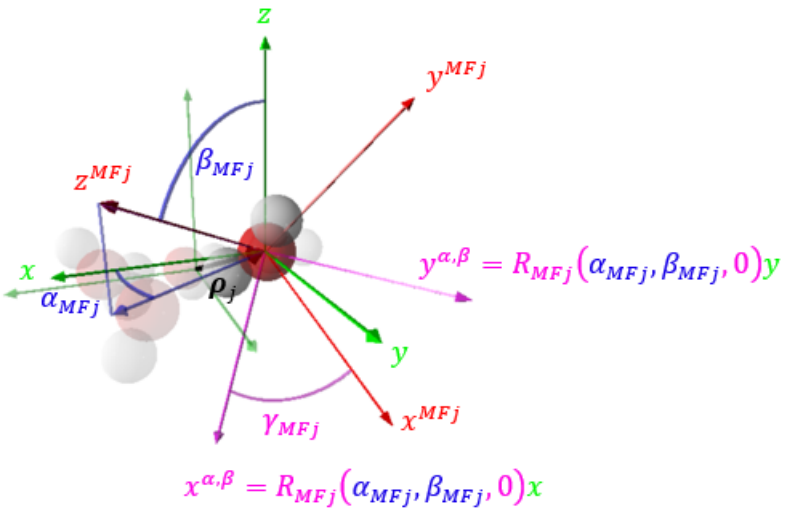

Figure 2.5: Illustration of the method of calculating the Euler angles α_{MFj}, β_{MFj}, γ_{MFj} for the j-th molecule in the cluster. The cluster frame is green, the molecular frame is red. The position vector of the molecule in the cluster frame $\boldsymbol{\rho_j}$ is black. The angles α_{MFj}, β_{MFj} are blue, the angle γ_{MFj} and the auxiliary molecular frame oriented without γ_{MFj} are magenta.

$R_{MFj}(\alpha_{MFj}, \beta_{MFj}, 0)$ is used to express the orientation of the molecular frame inside the cluster frame without the rotation by γ_{MFj}:

$$\begin{aligned} \boldsymbol{x}^{\alpha,\beta} &= R_{MFj}(\alpha_{MFj}, \beta_{MFj}, 0)\boldsymbol{x}, \\ \boldsymbol{y}^{\alpha,\beta} &= R_{MFj}(\alpha_{MFj}, \beta_{MFj}, 0)\boldsymbol{y}, \\ \boldsymbol{z}^{\alpha,\beta} &= R_{MFj}(\alpha_{MFj}, \beta_{MFj}, 0)\boldsymbol{z}, \end{aligned} \tag{2.26}$$

where $\boldsymbol{x}^{\alpha,\beta}$, $\boldsymbol{y}^{\alpha,\beta}$, $\boldsymbol{z}^{\alpha,\beta}$ are the basis vectors of this auxiliary molecular frame rotated only by $R_{MFj}(\alpha_{MFj}, \beta_{MFj}, 0)$ (see figure 2.5). After that, to calculate the angle γ_{MFj}, it must be distinguished whether γ_{MFj} is greater than or less than π. To do that, we calculate the angle between the x^{MFj} basis vector and the vector $x^{\alpha,\beta}$, which we denote γ_{check1}, and the angle between x^{MFj} and the $y^{\alpha,\beta}$ vector, denoted γ_{check2}. These angles are then used in an if statement calculating the angle γ_{MFj} as:

$$\gamma_{MFj} = \begin{cases} \gamma_{check1}, & \gamma_{check2} \leq \frac{\pi}{2}, \\ 2\pi - \gamma_{check1}, & \gamma_{check2} > \frac{\pi}{2}. \end{cases} \tag{2.27}$$

All these calculations are performed in the cluster frame. We have explicitly tested the correctness of this approach by reproducing the cluster geometries starting from the molecules in the molecular frame.

A visualization of the lowest energy cluster geometries from Rakshit et al. [2019b] for $(H_2O)_n$ clusters with $3 \leq n \leq 22$ is shown in figure 2.6.

2.4.2 Convergence with angular momentum for clusters

First of all, we tested the convergence of $\sigma(E)$ and $\beta_2(E)$ with the angular momentum l for the lowest-energy structures from Rakshit et al. [2019b] resulting

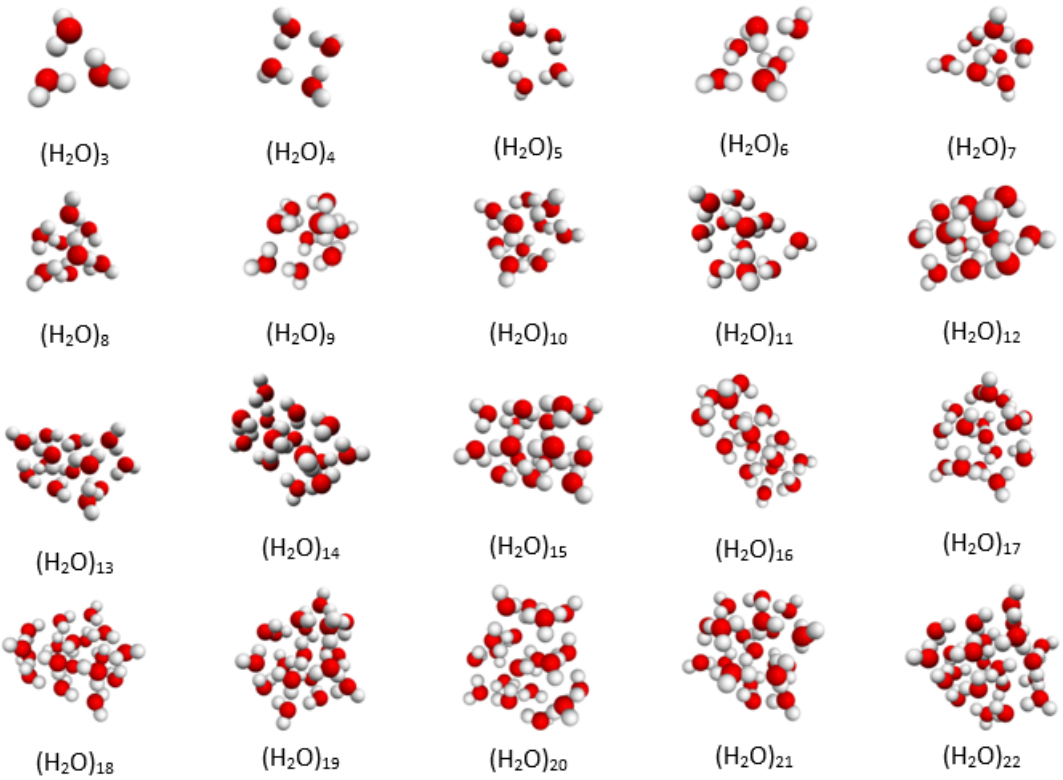

Figure 2.6: Visualizations of the putative structures of the $(H_2O)_n$ clusters for $3 \leq n \leq 22$ from the database on Rakshit et al. [2019b]. All these pictures correspond to the lowest energy structures from the results of the TTM2.1-F Potential method with the energy range 1.0 KJ/mol above the minimum (Rakshit et al. [2019a], Rakshit et al. [2019b]). Each picture is scaled independently.

from the TTM2.1-F method (Rakshit et al. [2019a]) with the range of 1.0 KJ/mol above the putative minimum for four clusters with $n = 3, \ldots, 6$. Note, that the distances in the files on Rakshit et al. [2019b] are given in Angstroms, hence we converted them to atomic units first. The results of the partial wave convergence test for the cluster with $n = 5$ molecules is exemplified in figure 2.7 and the results for other clusters ($n = 3, 4, 5$) are in figure A.1 in Attachment A.1.

From these figures it is clear that for all the tested clusters the main contribution is that of $l = 2$ and all the higher angular momenta give only corrections. That is expected since our independent molecule model reconstructs the dipoles of the individual molecules in their molecular frames: we have shown in Section 2.3 that the photoelectron angular distribution for a single molecule is also well converged for $l = 3$. With this result, despite we had the dipoles up to $l = 6$, we decided to use:

$$l \leq l_{max} = 3, \tag{2.28}$$

for all other calculations, which significantly decreased the computational demands.

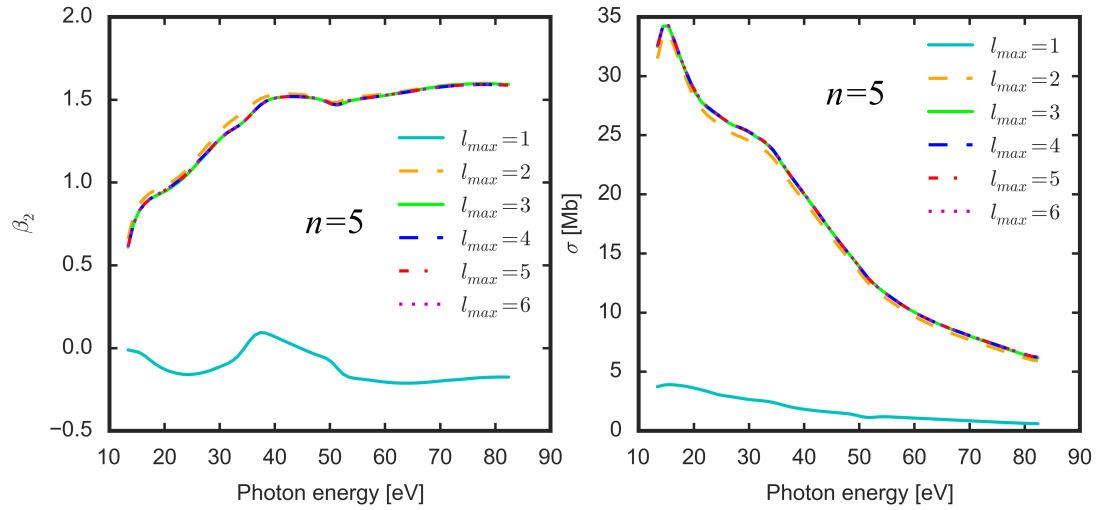

Figure 2.7: Results of the test of convergence of the IMM results with l for the $(H_2O)_5$ cluster. Left panel: β_2, right panel: σ. The results were calculated for the lowest energy structures from Rakshit et al. [2019b] resulting from the TTM2.1-F method (Rakshit et al. [2019a]) with energies up to 1.0 KJ/mol above the minimum.

2.4.3 Effects of the number of molecules

Motivated by the experimental results of Hartweg et al. [2017], we tested the effects of the number of constituent molecules on the photoelectron angular distribution for the clusters within the IMM. The results are shown in figure 2.8 for clusters with $n = 3, \ldots, 10$ monomers.

While the calculated cross sections $\sigma(E)$ systematically increase with the in-

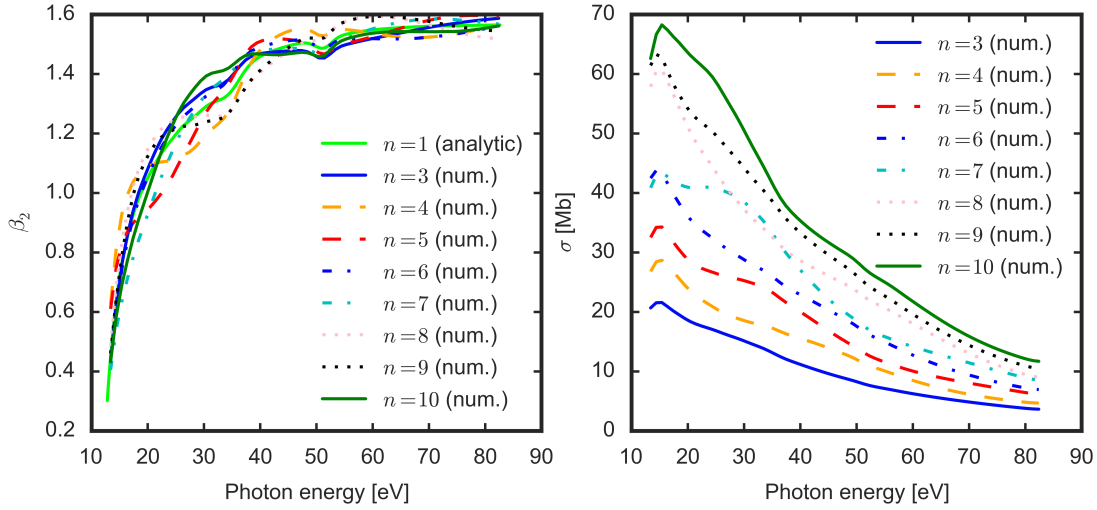

Figure 2.8: Effect of the number of molecules on the IMM results for clusters with $n = 3, \ldots, 10$ molecules. The β_2 parameters (left panel) for the clusters are compared with that for a single molecule. The results were calculated for the lowest-energy structures from Rakshit et al. [2019b] resulting from the TTM2.1-F method (Rakshit et al. [2019a]) with energies up to 1.0 KJ/mol.

creasing number of monomers in the clusters, the $\beta_2(E)$ parameters within our model do not exhibit the systematic decrease as measured by Hartweg et al. [2017] (cf. figure 1). Instead, the β_2 parameters for clusters in figure 2.8 oscillate around the value for a single molecule and the same trend continues also for higher n. This suggests, that the interference of partial waves from multiple ionized molecules in the cluster is not the main reason for the decrease of the experimental asymmetry parameters. The convergence of the β_2 around $n \sim 5$ observed by Hartweg et al. [2017] might therefore be caused mainly by the multiple scattering of the photoelectrons in the field of the cluster and by the change of the shape of the molecular orbitals due to the intermolecular interactions and charge redistribution in the cluster, which the IMM neglects and which are the other two reasons for the decrease of β_2 suggested by Hartweg et al. [2017]. However, the IMM results suggest that the interference of the photoionization amplitudes is responsible for modulation of the shape of the β_2 parameter, in particular in the region between 20-40 eV.

2.4.4 Effects of the geometric structure of the clusters

Following the study of the trends with the increasing number of monomers in the cluster, we move to the next topic which is investigating the effects of the geometry of the clusters and discussing the sensitivity of the photoelectron spectroscopy to the different conformations of the clusters calculated by Rakshit et al. [2019a].

Effects of different cluster conformations

To test the effects of the geometry of the clusters on the photoelectron angular distribution we used different geometries obtained from the database Rakshit et al. [2019b]. The paper Rakshit et al. [2019a] presents results of two methods for determining the possible structures of water clusters: (a) the TTM2.1-F Potential method, (b) the MP2/aug-cc-pVTZ method. A detailed description of those methods is beyond the scope of this work.

Method (a) has been used to determine putative geometries (local minima) of water clusters in three different energy ranges: 1.0 KJ/mol, 1.0 Kcal/mol, 5.0 Kcal/mol.[1] The structures from the lowest-energy range up to 1.0 KJ/mol have been used for most calculations presented here. For each cluster size starting from $n = 5$ the method gives several possible structures (local minima). For $n = 3$ and $n = 4$ only a single geometry is given in this energy range. Method (b) has been used by Rakshit et al. [2019a] to determine putative geometries of the lowest-energy structures only.

The effect of conformation on the photoelectron spectra was tested comparing results for the different conformations obtained using the method (a). Only in case of $n = 3$ and $n = 4$, where method (a) gives only a single structure, we used for $n = 3$ also the geometry obtained from method (b) and for $n = 4$ we used the structure from the method (a) from the third energy range up to 5.0 Kcal/mol.

All results of these tests are shown in comparison with the experimental results from Hartweg et al. [2017] and the analytic results for a single molecule in figures A.2 and A.3 in Attachment A.1. Here we present the results for the

[1] 1 KJ/mol = 0.01036427 eV, 1 Kcal/mol = 0.04336410 eV

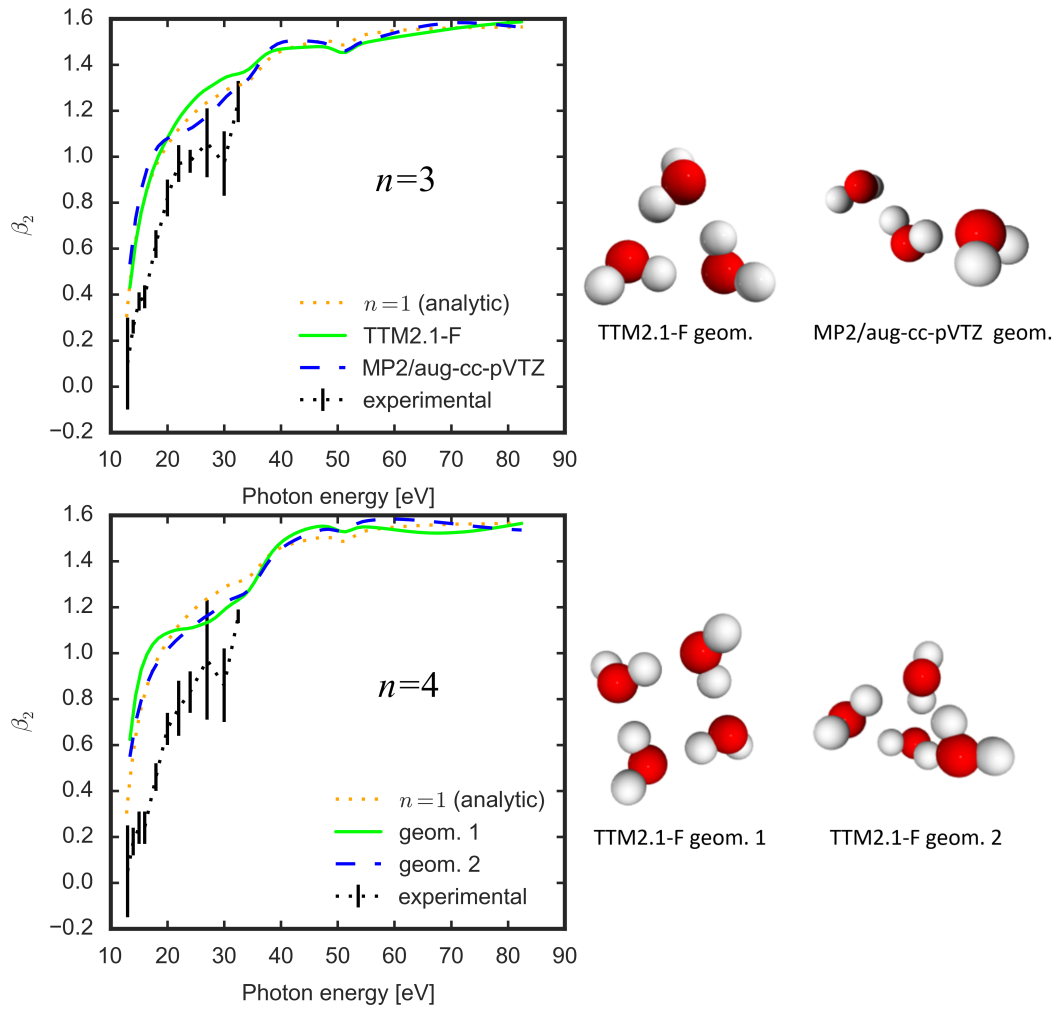

Figure 2.9: Calculated β_2 parameters for the conformations of the $(H_2O)_3$ and $(H_2O)_4$ clusters from Rakshit et al. [2019b] and their comparison with experimental results from Hartweg et al. [2017] and analytic result for a single molecule. The structures are shown in the right panel. The geometries of $(H_2O)_3$ result from the MP2/aug-cc-pVTZ method and the TTM2.1-F Potential method within the range of 1.0 KJ/mol above the minimum. The structures of $(H_2O)_4$ result from the TTM2.1-F Potential method within the range of 5.0 Kcal/mol above the minimum (Rakshit et al. [2019a]).

$\beta_2(E)$ asymmetry parameter for clusters $(H_2O)_3$ and $(H_2O)_4$ in figure 2.9 and for $(H_2O)_5$ and $(H_2O)_6$ in figure 2.10, all of these also in comparison with Hartweg et al. [2017] and the single molecule. The right panels of these figures show visualizations of the used geometries from Rakshit et al. [2019b].

Similarly as the results of testing the effects of the number of molecules n within our IMM (cf. fig. 2.8), the results here oscillate around the analytic values for a single molecule. Nevertheless, the shape of the curves for the individual cluster geometries differ from that for a single molecule and from each other. Only the results for the 1st and 3rd geometry of the $(H_2O)_5$ cluster seem to be very close to each other, yet not identical. This is probably because these structures differ only by small differences in the angles γ^{MFj} (rotations about the

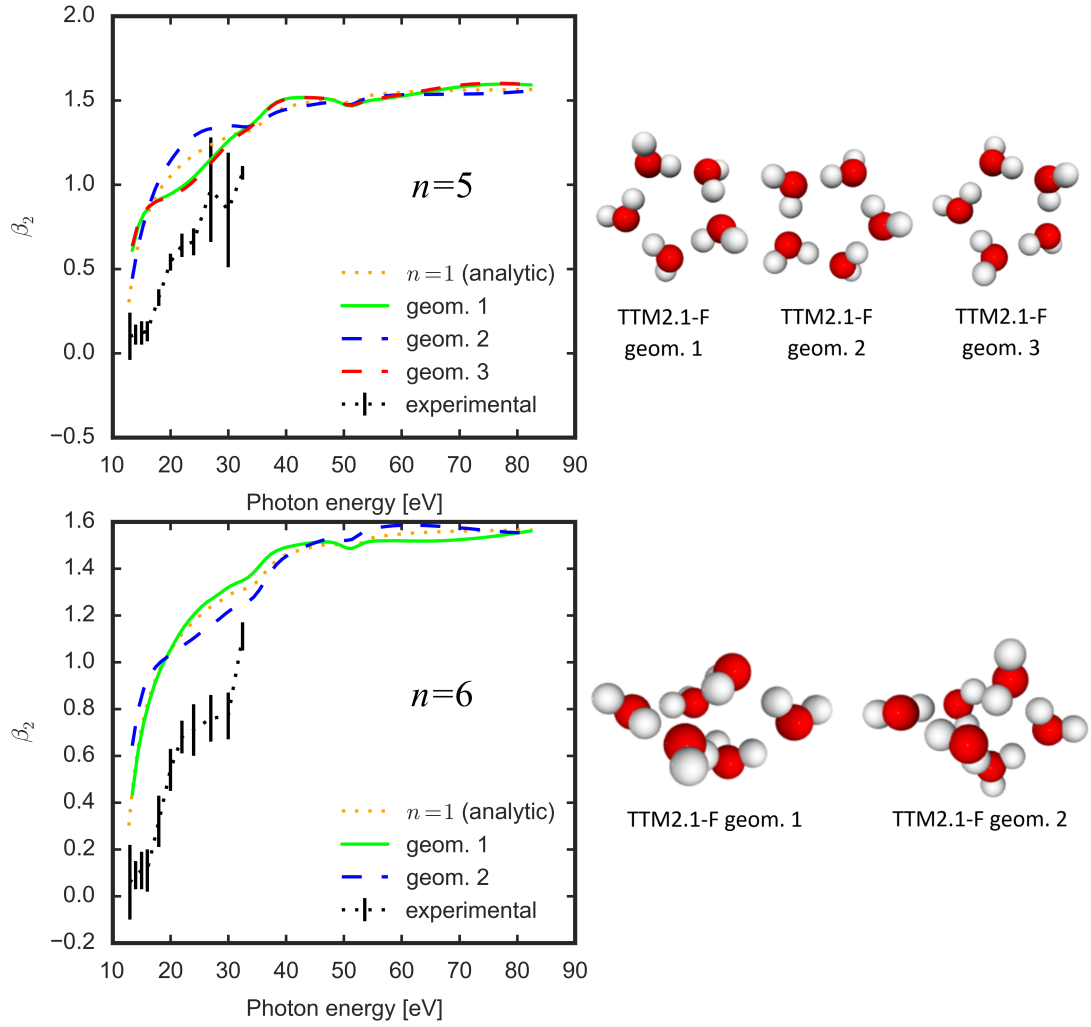

Figure 2.10: Calculated β_2 parameters for the conformations of the $(H_2O)_5$ and $(H_2O)_6$ clusters from Rakshit et al. [2019b] and their comparison with experimental results from Hartweg et al. [2017] and analytic result for a single molecule. The cluster structures are shown in the right panel. All these geometries result the TTM2.1-F Potential method within the range of 1.0 KJ/mol above the minimum (Rakshit et al. [2019a]).

mol-frame z^{MFj} axes) of a few of their molecules which means that in both cases the p-type $1b_1$ ionizing orbitals maintain approximately the same orientations.

These results mean that within the independent molecule model the photoelectron angular distribution is affected by the exact geometry. And moreover, our results provide a qualitative correspondence with the experiment of Hartweg et al. [2017]. Even though quantitatively our theory does not match the experimental results, the shape of the experimental curves of the β_2 parameter (especially the decrease at around 20-30 eV) is qualitatively reproduced for some of the cluster conformations. This suggests that the photoelectron spectroscopy might be a sensitive probe of the geometric structures of small water clusters. Interesting is, that in some cases ($n = 3, 4$) this correspondence with Hartweg et al. [2017] occurs for the second lowest-energy structure according to Rakshit et al. [2019b]. The reason for this might be that the structure of the clusters prepared

in the experiments does not correspond to the lowest-energy one or is mixture of different conformations within clusters with the same number of molecules.

Effects of distances of molecules from the origin

The effect of the distances ρ_j of the molecules from the cluster-frame origin was tested on the lowest-energy structures from Rakshit et al. [2019b] for clusters with $n = 3, \ldots, 6$ molecules in which we only scaled the distances of the molecules from the center of mass of the cluster. Here we present the result for $n = 4$ in figure 2.11. The other results are shown in figure A.4 in the Attachment A.1. The results were calculated for the distances $1.0\rho_j,\ 1.1\rho_j,\ 1.2\rho_j, \ldots,\ 2.0\rho_j$, however in order to preserve clarity of the figures we present only every second step of the scaling $(1.0\rho_j,\ 1.2\rho_j, \ldots,\ 2.0\rho_j)$.

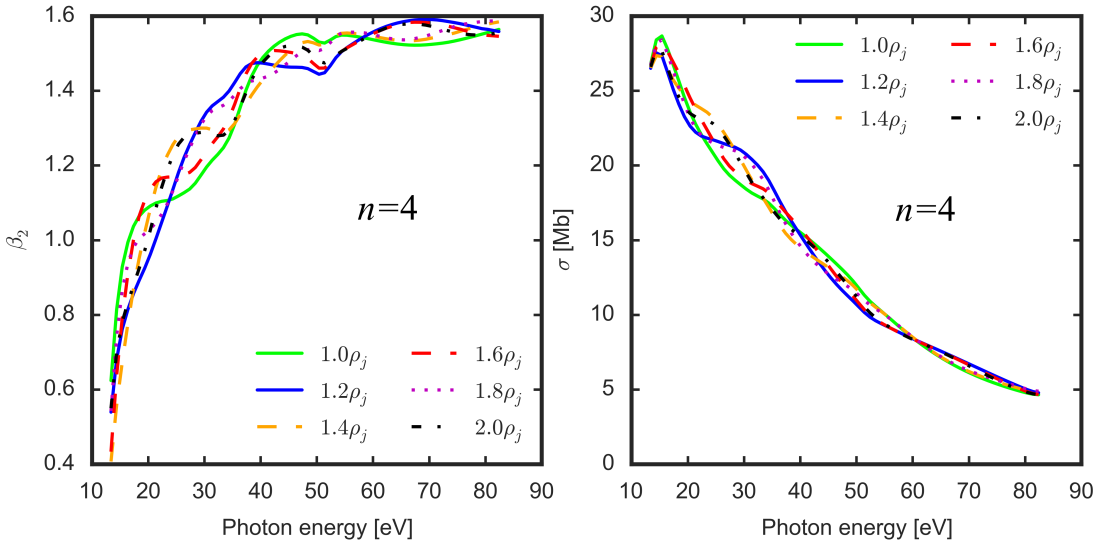

Figure 2.11: Effect of the distances of the molecules from the origin of the cluster frame ρ_j in the independent molecule model for the $(H_2O)_4$ cluster. The geometry for $1.0\rho_j$ is the lowest energy structure from Rakshit et al. [2019b] resulting from the TTM2.1-F Potential method.

The results in fig. 2.11 and fig. A.4 clearly differ for each different scale of ρ_j. The differences are more significant in case of the β_2 parameters but they are present also in the cross sections σ. This shows that within the IMM the asymmetry parameters and the cross sections are affected not only by the number of molecules n but also by the overall size of the clusters with the same n. This result may have implications for inclusion of the vibrational motion of the clusters.

2.4.5 Inconsistency of the analytic result using the available dipoles

The reason why the numerical calculation works correctly is that the spherical harmonics defined on each molecule are not coupled together. Instead, the full momentum-space dipoles are calculated for each molecule and coherently combined. The problem with the analytic calculation is the presence of spherical

harmonics in the partial wave dipoles which must be translated in order to perform the averaging, as explained in Subsection 1.3.2. This was verified explicitly by setting all the translation vectors $\boldsymbol{\rho_j}$ to $\vec{0}$ which gave an agreement between the analytic and the numerical results.

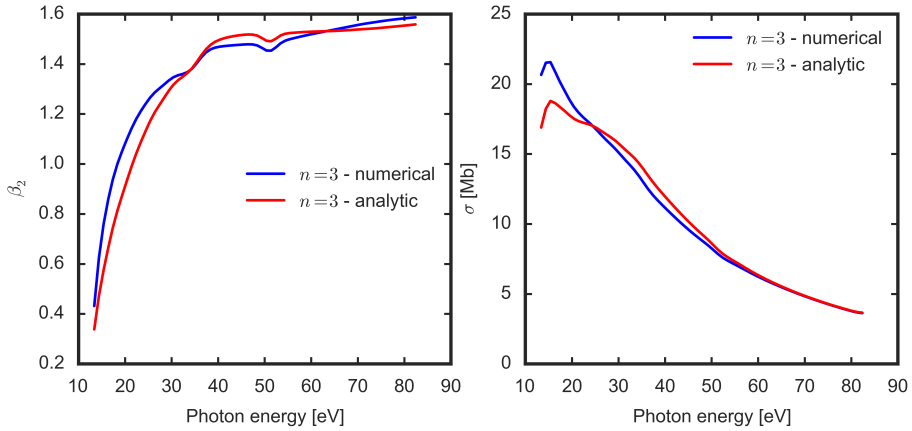

Figure 2.12: Comparison of the correct numerical results and incorrect analytic results for the cluster $(H_2O)_3$. The results were calculated for the lowest-energy structure of $(H_2O)_3$ from Rakshit et al. [2019b] resulting from the TTM2.1-F Potential method.

The difference between the numerical and the incorrect analytic results is shown in figure 2.12 for the lowest-energy $(H_2O)_3$ structure from Rakshit et al. [2019b]. For larger numbers of molecules the inconsistency of the analytic calculation using the improper dipoles was mostly increasing.

2.5 Discussion of the results

The analytic results for a single molecule in comparison with the numerical results and with the reference data obtained by my supervisor from the code UKRmol+ verify that the relations (1.72)-(1.76) for a single molecule are correct. The analytic formulae for clusters, however, could not be used for calculations correctly because of the unavailability of the partial wave dipole matrix elements in the basis of solid spherical harmonics. Nevertheless, the results for small water clusters were obtained numerically using an adaptive quadrature method as described in Section 2.2.

The tests of our independent molecule model on some of the putative geometries of water clusters from Rakshit et al. [2019b], presented in Section 2.4, suggest that the IMM may be able to at least qualitatively describe some of the recent experimental results from Hartweg et al. [2017] and that the photoelectron angular distribution might be sensitive to the geometry of the clusters.

Figures 2.9-2.11 and figures A.2-A.4 show that the IMM asymmetry parameters β_2 and cross sections σ differ depending on the conformation of the water cluster. Figures 2.9-2.10 and A.2-A.3 show even that the results of the IMM for some cluster structures qualitatively match the shape of the experimental results from Hartweg et al. [2017].

On the other hand, the results of the independent molecule model do not exhibit the systematic decrease of β_2 with the increasing number of molecules which was observed by Hartweg et al. [2017]. Since the IMM uses the partial wave expansion of the monomer states and neglects the charge redistribution in the cluster and multiple scattering of the released photoelectrons from the field of the cluster, this might mean that the decrease of the asymmetry parameter is caused mostly by the multiple scattering or by changes of the molecular orbitals, as proposed by Hartweg et al. [2017], and the effect of the interference of the partial waves from multiple photoionization centers is weak in comparison with these two phenomenons.

Our results therefore suggest that the direct interference of photoionization amplitudes is responsible for the modulation of the shape of the β_2 parameters while the multiple scattering for their overall magnitudes. Nevertheless, the IMM results need to be carefully compared to accurate calculations before this hypothesis can be confirmed.

Conclusion

We have developed an approximate independent molecule model of molecular cluster photoionization and used it to investigate some aspects of the single photon ionization of small water clusters.

First we derived formulae for β-parameters and cross section for photoionization of a gas of randomly oriented molecules. We then generalized this approach to the IMM of ionization of molecular clusters. This model is applicable to both homogeneous and heterogeneous clusters.

I have developed Python codes for evaluation of the analytic formulae for a single molecule and rewritten it in FORTRAN for the formulae for clusters and we have extended an existing FORTRAN numerical code for a single molecule molecule to the case of clusters.

Unfortunately, the analytic formula for the photoelectron angular distribution, which is the main theoretical result of our IMM model, could not be properly tested due to the absence of the partial wave dipole matrix elements in the basis of solid harmonics. In order to generate the dipoles in this basis of solid harmonics, changes of the UKRmol+ code would be needed. Nevertheless, we used at least the equivalent numerical approach and applied it on the putative geometries of the small water clusters from Rakshit et al. [2019b].

Although our results do not exhibit the observed decrease of the experimental asymmetry parameters with the increasing number of molecules in the clusters, they do show some qualitative correspondence with the recent experiments. The β_2 parameters calculated for some cluster conformations have similar shape as the experimental curves. This suggests that direct interference of photoionization amplitudes may modulate the shape of the β_2 parameters while the multiple scattering may be the main effect affecting the overall magnitudes of β_2. The differences between the asymmetry parameters and cross sections calculated for different conformations of the clusters of the same size also suggest that the photoionization spectra are sensitive even to small changes of the geometry of the clusters. This might mean that the photoelectron spectroscopy could potentially be used to study or verify the geometric structures of the small water clusters experimentally. However, further research, using e.g. the R-matrix method, see Mašín et al. [2020], is needed to study the validity of our model before its results can be interpreted conclusively.

Bibliography

A.-R. Allouche. Gabedit — A graphical user interface for computational chemistry softwares. *Journal of Computational Chemistry*, 32(1):174–182, 2011.

M. A. Blanco, M. Flórez, and M. Bermejo. Evaluation of the rotation matrices in the basis of real spherical harmonics. *Journal of Molecular Structure (Theochem)*, 419:19–27, 1 1997.

D. M. Brink and G. R. Satchler. *Angular Momentum*. Oxford University Press, Oxford, 2nd edition, 1968.

S. Caprasecca. *Theoretical studies of low energy electron collisions with small molecular clusters*. PhD thesis, The Open University, 9 2010.

A. W. Jr. Castleman and P. Jena. Clusters: A bridge across the disciplines of environment, materials science, and biology. *Proceedings of the National Academy of Sciences USA*, 103(28):10554–10559, 2006.

P. Cejnar. *A Condensed Course of Quantum Mechanics*. Karolinum, Prague, 1st edition, 2013. ISBN 978-80-246-2321-4. Handbook for a course of quantum mechanics at Faculty of Mathematics and Physics, Charles University.

N. Chandra. Photoelectron spectroscopic studies of polyatomic molecules. I. theory. *Journal of Physics B: Atomic and Molecular Physics*, 20(14):3405–3415, 1987.

A. I. Dragan, D. J. Russell, and P. L. Privalov. DNA hydration studied by pressure perturbation scanning microcalorimetry. *Biopolymers*, 91(1):95–101, 2009.

W. W. Duley. Molecular Clusters in Interstellar Clouds. *The Astrophysical Journal*, 118(1):L57–L60, 1996.

U. Fano. Propensity rules: An analytical approach. *Physical Review A*, 32: 617–618, Jul 1985.

M. Faubel, K. R. Siefermann, Y. Liu, and B. Abel. Ultrafast Soft X-ray Photoelectron Spectroscopy at Liquid Water Microjets. *Accounts of Chemical Research*, 45(1):120–130, 2012.

T. C. Freitas, M. A. P. Lima, S. Canuto, and M. H. F. Bettega. Electron collisions with the CH_2O-H_2O complex. *Physical Review A*, 80:062710, 2009.

H. Friedrich. *Theoretical Atomic Physics*. Springer, New York, Berlin, Heidelberg, 3rd edition, 2006. ISBN 978-3-540-25644-1.

M. Fárník. *Molecular Dynamics in Free Clusters and Nanoparticles Studied in Molecular Beams*. Institute of Chemical Technology, Prague, 2011. ISBN 978-80-7080-781-1. DSc. thesis, e-book available at http://vydavatelstvi.vscht.cz/.

R. G. Harrison and K. S. Carslaw. Ion-aerosol-cloud processes in the lower atmosphere. *Reviews of Geophysics*, 41(3):1012, 2003.

S. Hartweg, B. L. Yoder, G. A. Garcia, L. Nahon, and R. Signorell. Size-Resolved Photoelectron Anisotropy of Gas Phase Water Clusters and Predictions for Liquid Water. *Physical Review Letters*, 118:103402, 2017.

T. Helgaker, J. Olsen, and P. Jorgensen. *Molecular Electronic-Structure Theory*. Wiley, 2000. ISBN 978-1-118-53147-1.

F. Huisken, M. Kaloudis, and A. Kulcke. Infrared spectroscopy of small size-selected water clusters. *The Journal of Chemical Physics*, 104:17, 1996.

R. L. Johnston. *Atomic and Molecular Clusters*. Taylor and Francis, London and New York, 2002. ISBN 0-203-48489-4 Master e-book ISBN. This edition published in the Taylor and Francis e-Library, 2005.

J. Kreil, M.-W. Ruf, H. Hotop, I. Ettischer, and U. Buck. Threshold electron attachment and electron impact ionization involving oxygen dimers. *Chemical Physics*, 239:459–473, 1998.

V. I. Lebedev. Quadratures on a sphere. *USSR Computational Mathematics and Mathematical Physics*, 16(2):10 – 24, 1976.

P. P. Man. Wigner active and passive rotation matrices applied to NMR tensor. *Concepts in Magnetic Resonance Part A*, 45A:e21385, 2017.

H. S. W. Massey, E. H. S. Burhop, and H. B. Gilbody. *Electronic and Ionic Impact Phenomena*, volume 2. At the Clarendon Press, Oxford, 2nd edition, 1969.

Z. Mašín, J. Benda, J. D. Gorfinkiel, A. G. Harvey, and J. Tennyson. UKRmol+: A suite for modelling electronic processes in molecules interacting with electrons, positrons and photons using the R-matrix method. *Computer Physics Communications*, 249:107092, 2020.

T. E. Morrell and G. C. Shields. Atmospheric Implications for Formation of Clusters of Ammonium and 1-10 Water Molecules. *Journal of Physical Chemistry A*, 114(12):4266–4271, 2010.

S. H. Nam, H. S. Park, J. K. Song, and S. M Park. Photoinduced Dynamics of Hydrated Adenine Clusters. *Journal of Physical Chemistry A*, 111(18):3480–3484, 2007.

I. Powis. Photoelectron circular dichroism of the randomly oriented chiral molecules glyceraldehyde and lactic acid. *The Journal of Chemical Physics*, 112(1):301, 2000.

A. Rakshit, P. Bandyopadhyay, J. P. Heindel, and S. S. Xantheas. Atlas of putative minima and low-lying energy networks of water clusters n = 3–25. *The Journal of Chemical Physics*, 151:214307, 2019a.

A. Rakshit, P. Bandyopadhyay, J. P. Heindel, and S. S. Xantheas. Database of Water Cluster Minima (total of 4,948,959 networks) for n=3-30, 2019b. URL `https://sites.uw.edu/wdbase/database-of-water-clusters/`. Last access 30 May 2020.

B. Ritchie. Theory of the angular distribution of photoelectrons ejected from optically active molecules and molecular negative ions. *The Journal of Chemical Physics*, 13(4):1411–1415, 1976.

S. Sen, D. Andreatta, S. Y. Ponomarev, D. L. Beveridge, and M. A. Berg. Dynamics of water and ions near DNA: comparison of simulation to time-resolved stokes-shift experiments. *Journal of the American Chemical Society*, 131(5): 1724–1735, 2009.

A. Trabattoni, L. Colaizzi, L. Ban, V. Wanie, Saraswathula K., E. P. Månsson, P. Rupp, Q. Liu, L. Seiffert, E. A. Herzig, A. Cartella, B. L. Yoder, F. Légaré, M. F. Kling, T. Fennel, R. Signorel, and F. Calegari. Photoelectron spectroscopy of large water clusters ionized by an XUV comb. *Journal of Physics: Photonics*, 2:035007, 2020.

D. A. Varshalovich, Moskalev A. N., and V. K. Khersonskii. *Quantum Theory of Angular Momentum*. World Scientific Publishing Co. Pte. Ltd., Singapore, 1988. ISBN 9971-50-996-2 pbk.

C. N. Yang. On the Agular Ddistribution in Nuclear Reactions and Coincidence Measurements. *Physical Review*, 74(7):764–772, 10 1948.

Y. Yonetani, Y. Maruyama, F. Hirata, and H. Kono. Comparison of DNA hydration patterns obtained using two distinct computational methods, molecular dynamics simulation and three-dimensional reference interaction site model theory. *The Journal of Chemical Physics*, 128(18):185102, 2008.

C. Zhang, T. Andersson, M. Förstel, M. Mucke, T. Arion, M. Tchaplyguine, B. Björneholm, and U. Hergenhahn. The photoelectron angular distribution of water clusters. *The Journal of Chemical Physics*, 138:234306, 2013.

List of Figures

A. Attachments

A.1 Additional figures

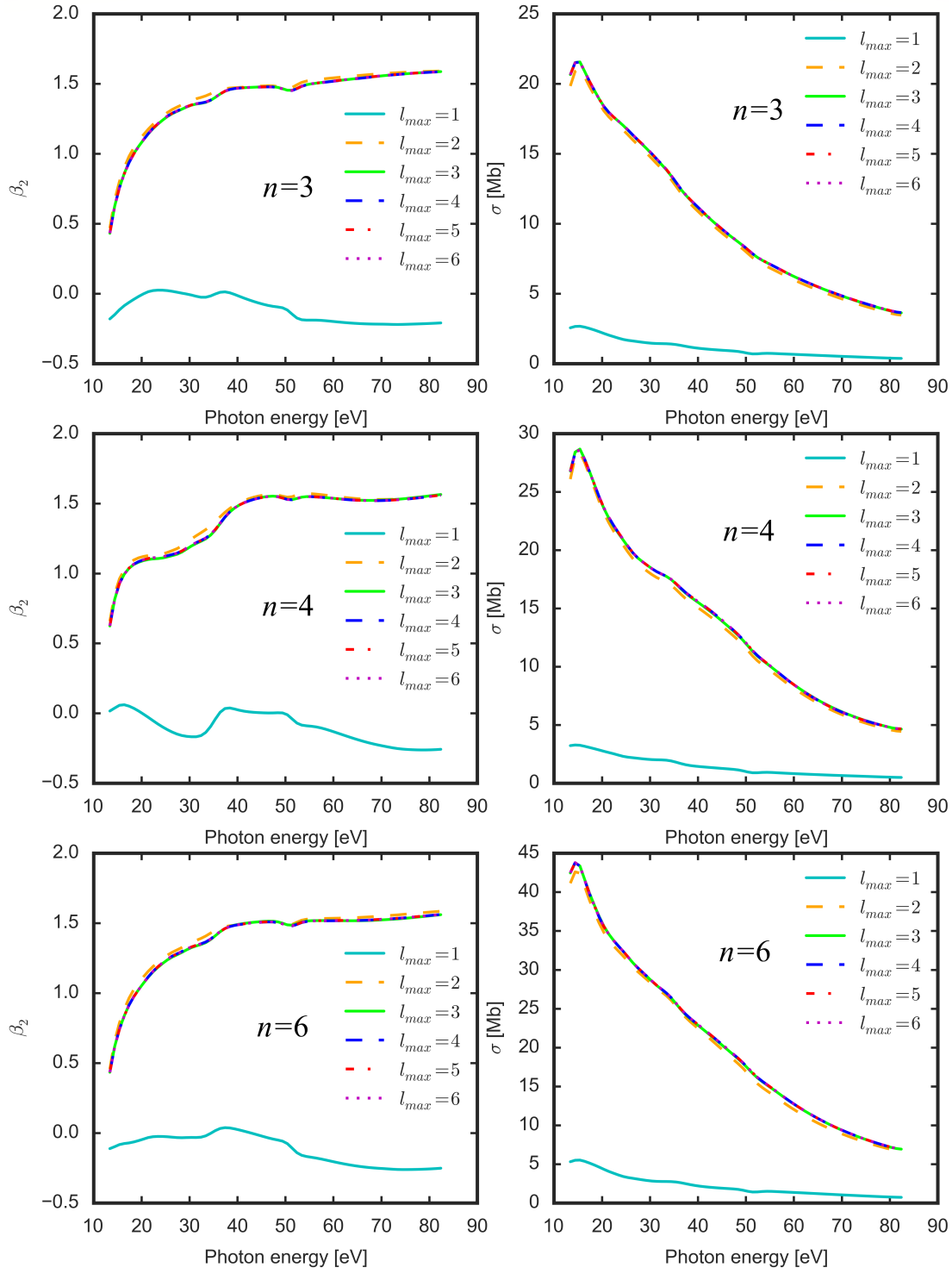

Figure A.1: Results of the test of convergence of the numerical calculation with l for the lowest-energy $(H_2O)_3$, $(H_2O)_4$ and $(H_2O)_5$ cluster structures from Rakshit et al. [2019b] from the TTM2.1-F Potential method.

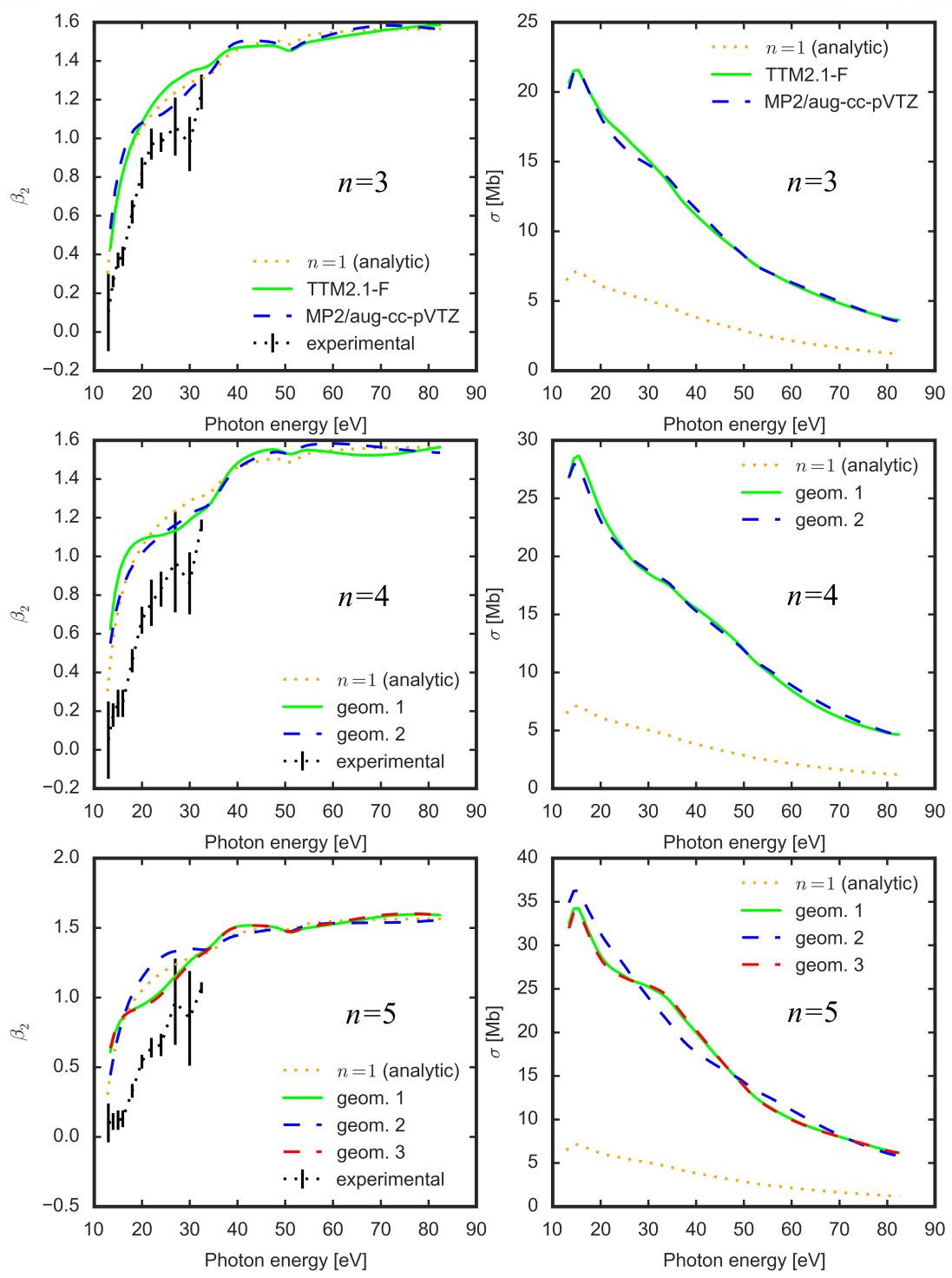

Figure A.2: Effect of the different conformations from Rakshit et al. [2019b] on the asymmetry parameter and the cross section for the $(H_2O)_3$, $(H_2O)_4$ and $(H_2O)_5$ clusters. The results of the IMM for clusters are compared with the experimental data from Hartweg et al. [2017] and with the analytic results for a single molecule. One geometry for $(H_2O)_3$ results from the MP2/aug-cc-pVTZ method, the others from the TTM2.1-F Potential method.

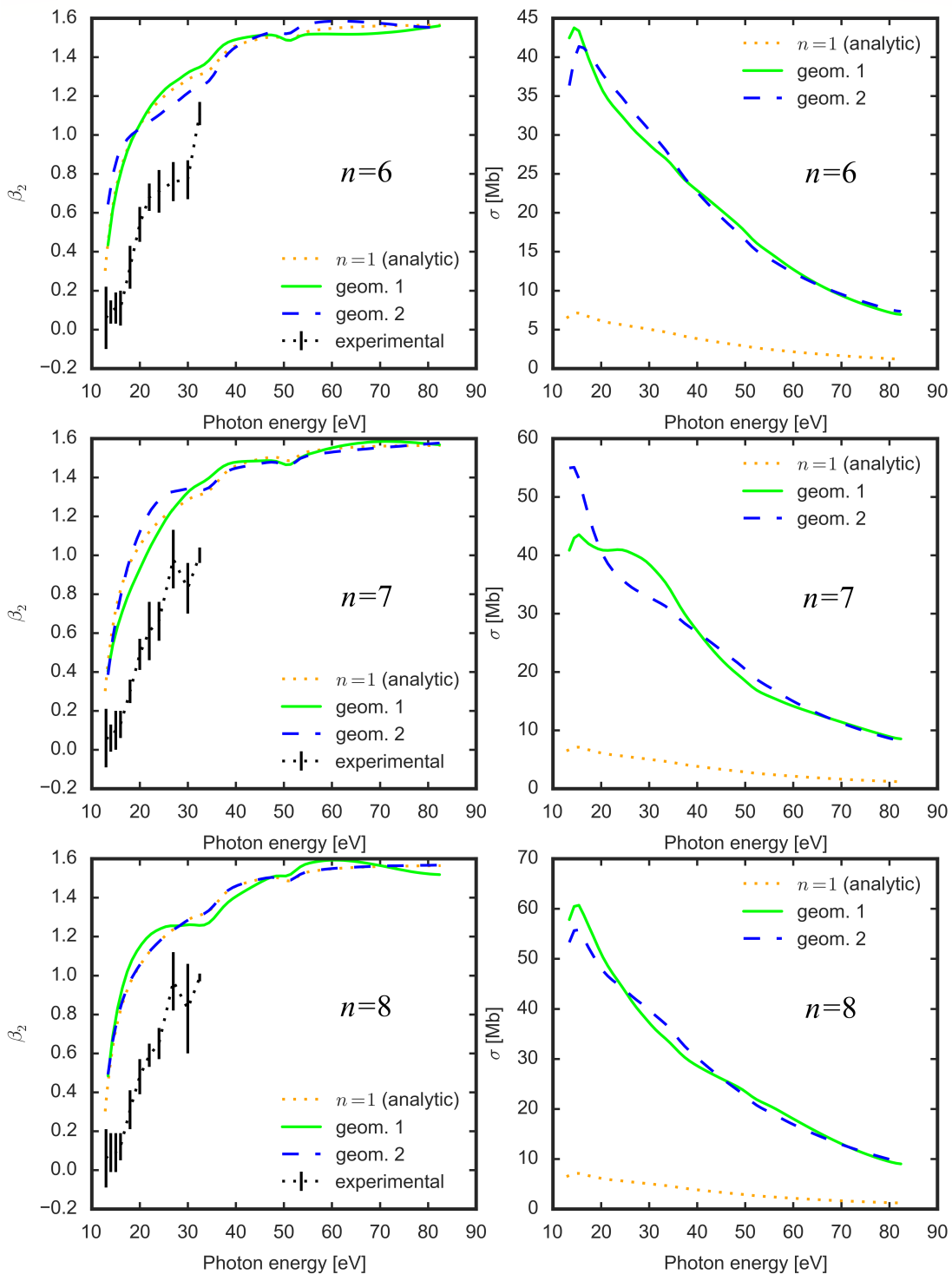

Figure A.3: Effect of the different conformations from Rakshit et al. [2019b] on the asymmetry parameter and the cross section for the $(H_2O)_6$, $(H_2O)_7$ and $(H_2O)_8$ clusters. The results of the IMM for clusters are compared with the experimental data from Hartweg et al. [2017] and with the analytic results for a single molecule. The geometries used come from the TTM2.1-F Potential method.

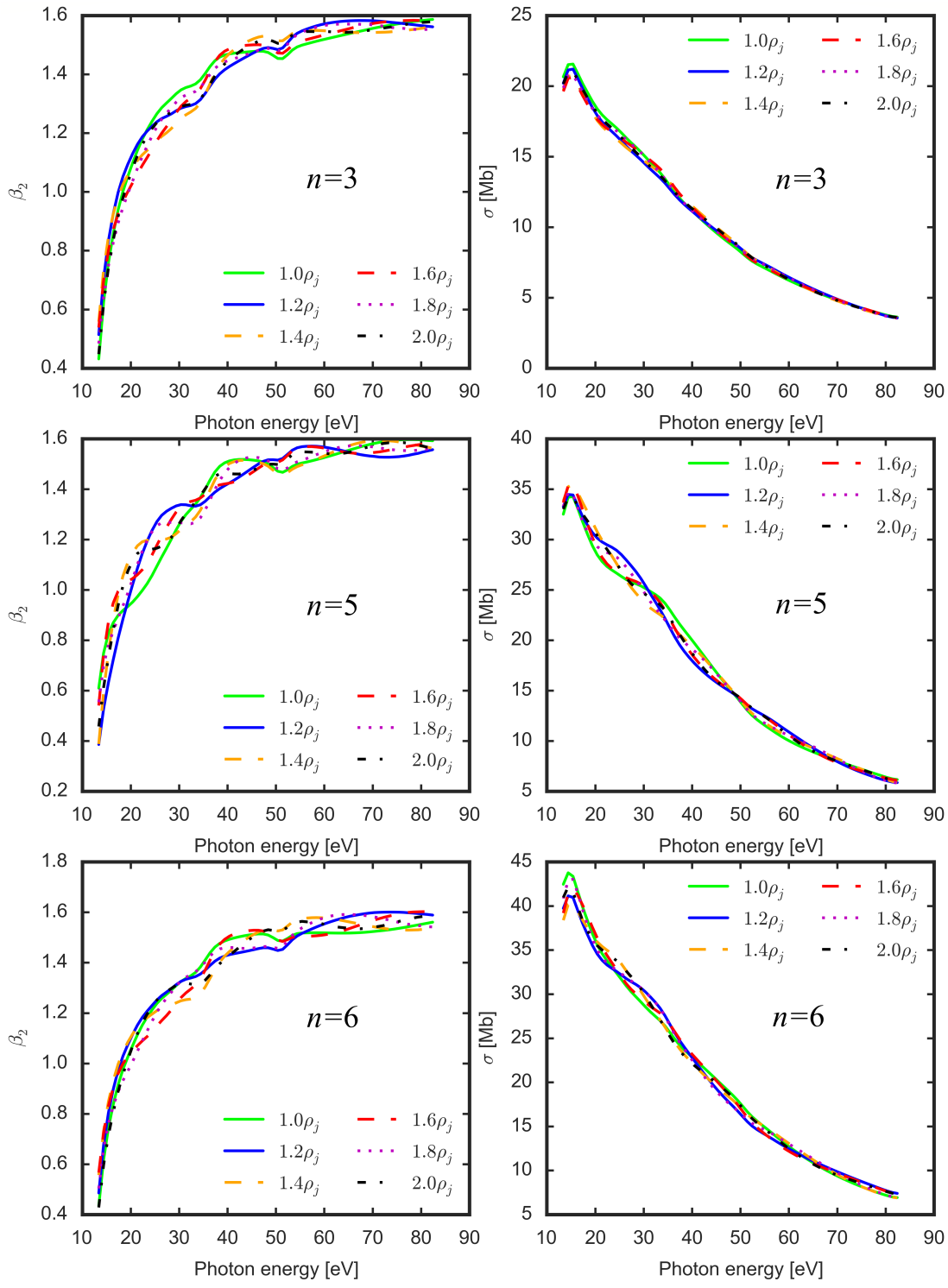

Figure A.4: Effect of the distances of the molecules from the origin of the cluster frame ρ_j in the independent molecule model for the $(H_2O)_3$, $(H_2O)_5$ and $(H_2O)_6$ clusters. The geometries for $1.0\rho_j$ are the lowest energy structures from Rakshit et al. [2019b] resulting from the TTM2.1-F Potential method.